The Cosmic Dust Analyser Data Handbook

Sascha Kempf, Ralf Srama, & Amara Graps

Contents

Contents

1. Introduction

The Cosmic Dust Analyser (CDA) (Srama et al., 2004) consists of two independent instruments: the High Rate Detector (HRD) and the Dust Analyser (DA). The HRD is designed to monitor high impact rates (up to $10^4 \mathrm{s}^{-1}$) in dust-rich environments such as during the Saturn ring plane crossings. The DA is sensitive to particles within a large mass range ($5 \cdot 10^{-18}$ kg $\ldots$ 10^{-12} kg for $v_d \approx 20 \mathrm{km\,s}^{-1}$) and velocity range ($1 \mathrm{km\,s}^{-1}$ $\ldots$ $100 \mathrm{km\,s}^{-1}$), and measures the charge carried by the dust grain, mass, impact velocity, and elemental composition of the impactor. This is accomplished by a suite of three detectors: a charge sensing unit (QP detector) in front of the instrument, a classical Impact Ionisation Detector (IID) similar to the Galileo-type dust detector, and a time-of-flight (TOF) mass spectrometer (Chemical Analyser - CA).

The scientific goals of the Cassini dust instrument were defined as:

Cruise Science Extend studies of interplanetary dust to the orbit of Saturn. Sample the chemical composition of dust in interplanetary space and across the asteroid belt. Determine the flux of interstellar particles during solar maximum conditions. Search for dust streams originating from Saturn.

Jupiter flyby Investigate the dynamics of the Io dust streams as discovered by Ulysses and Galileo. Characterise their direction, size-mass-distribution and correlation with the jovian and interplanetary magnetic field. Investigate the dust stream fluxes caused by the jovian system with respect to the Jupiter distance. Analyse dust stream particles at a different epoch from Galileo. Characterise the elemental composition of dust stream particles.

Rings Map size distribution of ring material, search for ring particles beyond the known E ring. Analyse the chemical composition of ring particles. Study dynamical processes (erosional and electromagnetic) responsible for the E ring structure, study interactions between the E ring and Saturns magnetosphere, search for electromagnetic resonances.Determine dust and meteoroid distribution both, in the vicinity of the rings and in interplanetary space.

Icy satellites Define the role of meteoroid impacts as mechanism of surface modifications. Obtain information on the chemical composition of satellites from the analysis of gravitationally bound ejecta particles in the vicinity of the satellites (within Hill spheres). Investigate interactions with the ring system and determine the importance of the various satellites as a source for ring particles.
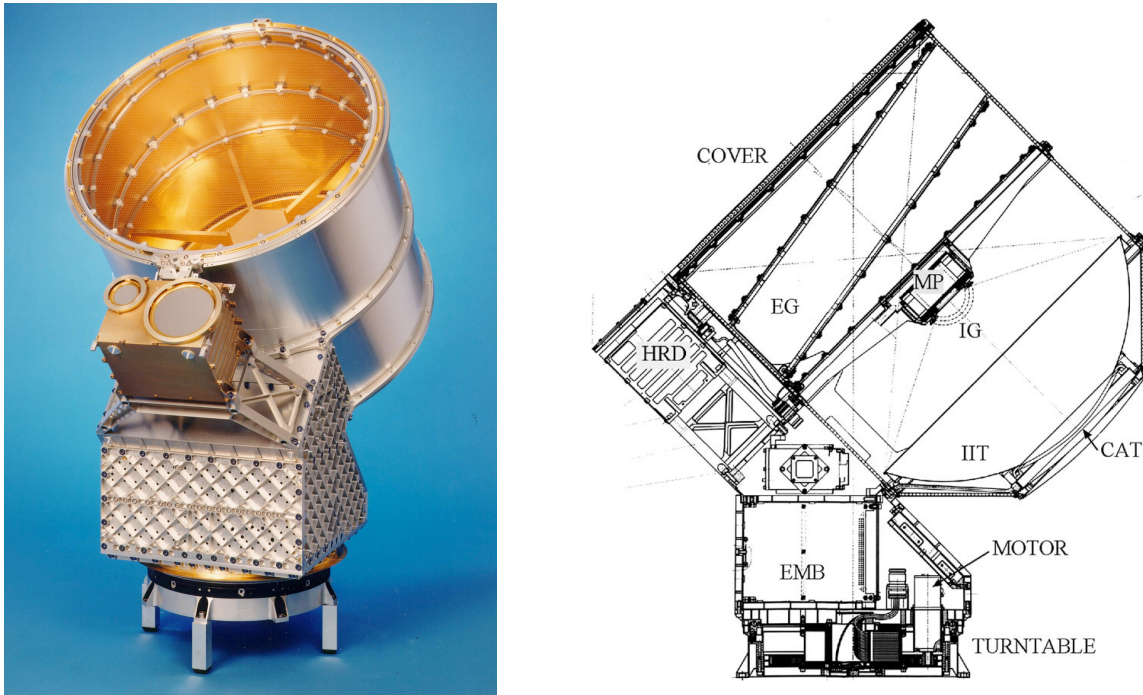
Figure 1.1.: The Cosmic Dust Analyser CDA. Left: image of the instrument before mounting onto the spacecraft. Right: technical drawing of the instrument. EG – entrance grids, IG – ion grids, EMB – electronics main box, IIT – impact ionisation target, CAT – chemical analyser target, MP – multiplier. The Impact Ionisation Detector (IID) is composed of the spherical impact target (IIT and CAT), the ion grids (IG), and the multiplier (MP). From Srama et al. (2004).

Magnetosphere of Saturn Determine the role that dust plays as source and sink of charged particles in the magnetosphere. Search for electromagnetically dominated dust (small particles) and for dust streams.

1.0.1. Impact Ionisation Detector - IID

1.1. Dust Analyser DA

The CDA impact ionisation detector subsystem (Srama et al., 2004) is similar to the detectors on the Galileo spacecraft (Grün et al., 1992b) and on the Ulysses spacecraft (Grün et al., 1992a). A high velocity impact on the hemispheric target transforms the striking dust particle into a mixture of particle fragments (ejecta) and an impact plasma. After separation in the electrical field, ions and electrons are collected by separate electrodes (see Fig. 1.2). Tests have shown that the time it takes the collected impact charge to rise to its maximum is independent of the impactor mass, and depends upon the impact velocity (Eichhorn, 1978). However, the impact charge is a function
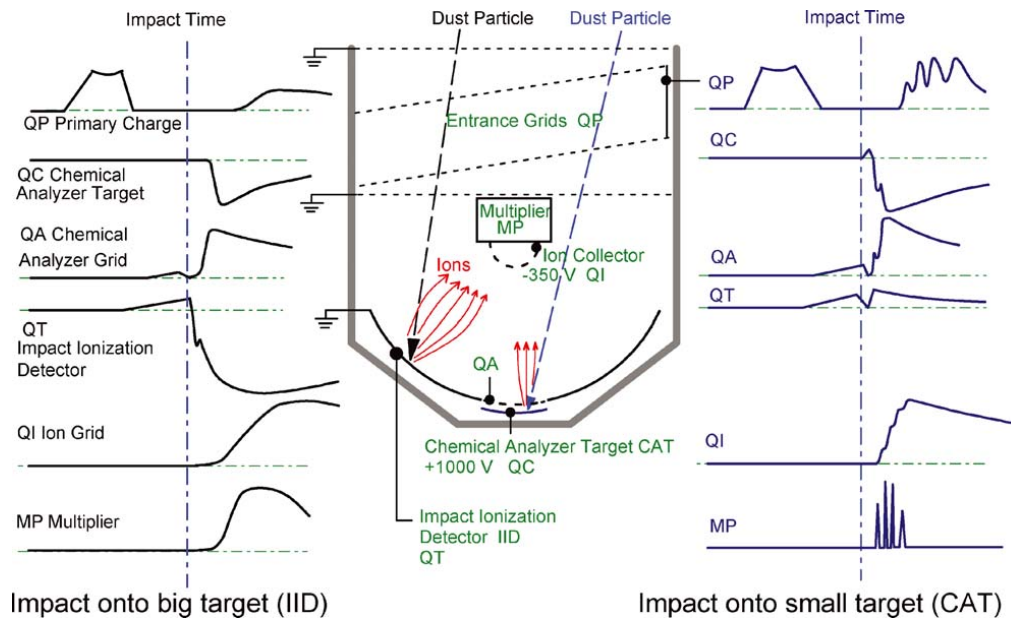
Figure 1.2.: Function principle of the CDA impact ionization detector DA. Shown are the signals caused by an impact on the Impact Ionisation Target IIT (left) and on the Chemical Analyzer Target CAT (right). From Srama et al. (2004).

of the impactor's mass as well as of the impact velocity.

The IID detector consists of an impact target and an ion grid system mounted in front of a multiplier (Fig. 1.1). Although the IID detector has inherited a lot from its progenitors, there are some important differences in its design. First of all, in order to integrate a TOF mass spectrometer into the IID, the spherical impact target was divided into an inner target made of rhodium (Chemical Analyser Target - CAT) and an outer target made of gold (Impact Ionisation Target - IIT). Both targets were attached to charge amplifiers (charge measured at the CAT: QC signal, charge measured at the IIT: QT signal). Furthermore, to ensure a high dynamic range of the target signals as well as of the ion grid signal QI, the measurement ranges were split. Depending on the amplitude of the target signal, the electronics switch the input source from a high sensitivity amplifier ($q \leq 10^{-11}$C) to a low sensitivity amplifier ($q \leq 10^{-8}$C). Unfortunately, the information about a performed range switch is not always transmitted to Earth, and must be deduced from the signal itself. The range switches may cause significant crosstalk between the various amplifiers, which degrades impact ionisation data of massive particles significantly.

The three impact ionisation signals are sampled continuously at 375 kHz until at least one of the signals exceeds the corresponding preset threshold. In this case, a measurement cycle is triggered and the sampling frequencies are increased (QT: 3 MHz,
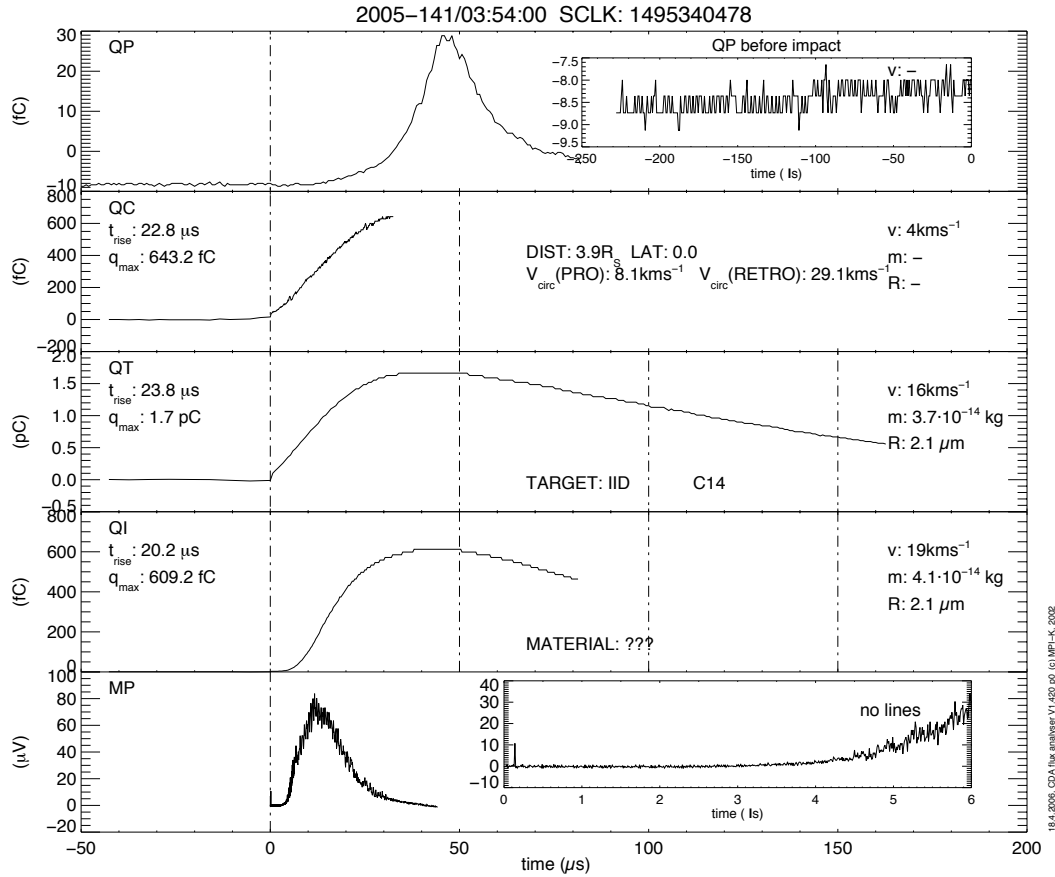
Figure 1.3.: DA signals caused by an impact of an approximately 2μm E ring particle on the IIT. The time axis is relative to the trigger time. The two target signals (QT and QC) and the ion grid signal (QI) rise until all available plasma charges are collected. Then, the charge amplifiers start to discharge $\sim \exp(-t/\tau)$. The inset in the uppermost panel shows the QP signal before the measurement was triggered. The pronounced bulge of the QP signal at about 50μs is due to escaping plasma ions which were not collected at the ion grid.

QC & QI: 6 MHz). To allow a comprehensive analysis of the signal slope, the last 16 samples preceding the trigger are stored together with the data taken afterwards. The signals are digitised with 8 bit resolution. Depending on the commanded instrument set-up, the signals may be further processed by the flight software (e.g. reduction of the signal length by a multiple of 2 - "shrinking", or lossy reduction of the signal's noise - "denoising"), which has to be considered for the data reduction. Fig. 1.3 and 1.4 show recorded signals of a typical impact on the IID and on the CAT, respectively.

2005−141/02:54:19 SCLK: 1495336897
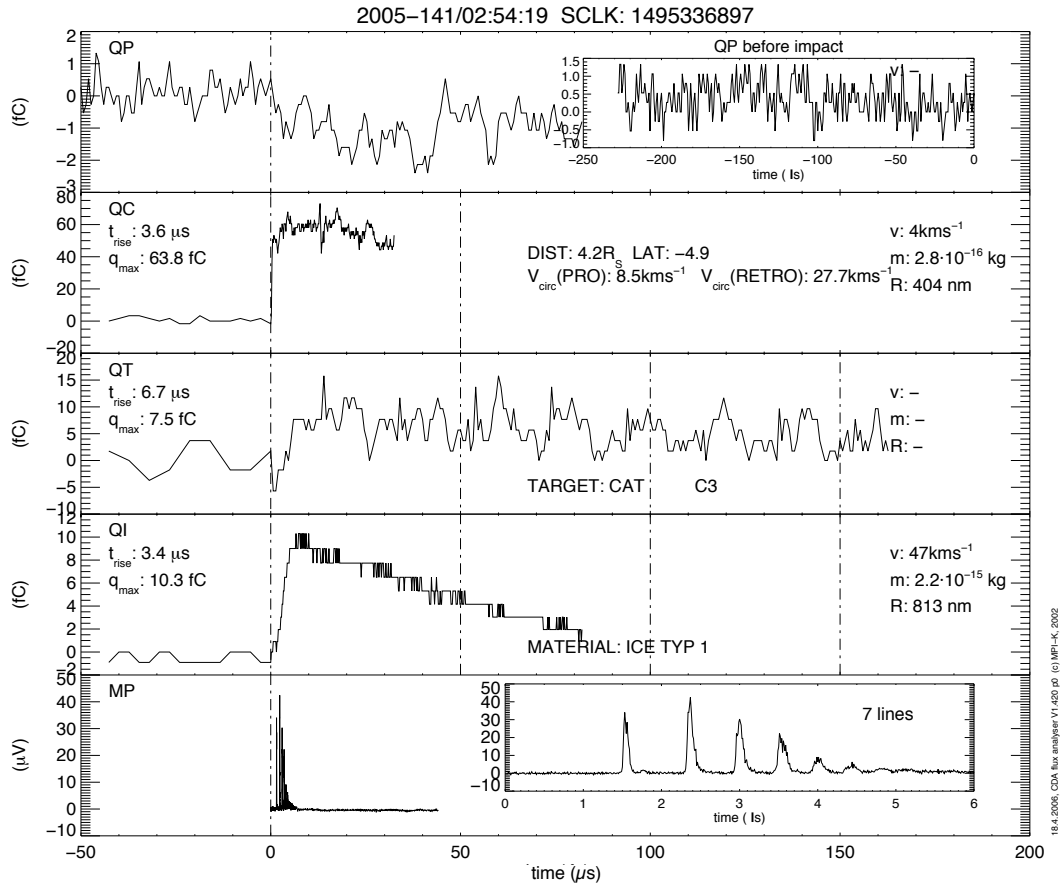
Figure 1.4.: DA signals caused by an impact of an approximately $0.5\,\mu m$ E ring particle on the CAT. The impact charge rise times are much shorter than for an impact on IIT of comparable speed due the strong electric field between the CAT and the acceleration grid ($\sim 330\,V/mm$). The inset in the lowermost panel shows the first $6\,\mu s$ of the MP signal corresponding with flight times of atomic species and light molecules. The shown time-of-flight mass spectrum is typical for a relatively slow impact of a water ice grain. The mass lines are due to water cluster ions $(H_2O)_i H_3O^-$ with $i \geq 0$.

1.1.1. Charge sensing unit - QP

The basic principle of the CDA charge detection system (QP detector) was developed and tested by Auer (1975). The dust charge is determined by measuring the charge the particle induces onto a shielded grid system in front of the dust detector. Fig. 1.5 gives a schematic view of the QP detector. A particle entering the instrument is flying on a straight trajectory through the charge detection unit until it hits the impact target at time t_{imp}. While flying between the shield grids (0, 3) a charged dust particle will induce its charge on the inner grids (1, 2) which are connected to a charge sensitive amplifier (QP signal). The amplified charge signal QP rises linearly as long as the par-
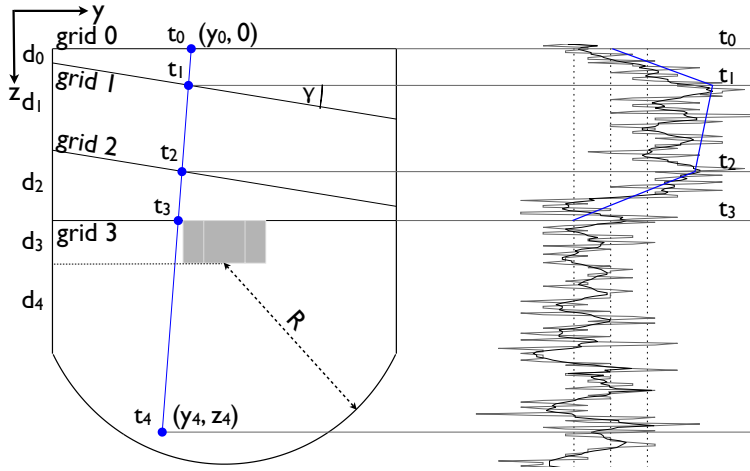
Figure 1.5.: The CDA charge detection system (Auer et al., 2002) consists of 4 grids
$(0 \cdots 3)$ mounted in front of the DA. The two inclined innermost grids (inclination angle $\gamma = 8.99°$) are connected to a charge sensitive amplifier
(QP signal), while the first grid and the last grid are grounded acting as
a Faraday cage. A particle penetrating the first grid at point 0 is hitting
the hemispheric target at point 4. The right plot shows the charge signal
induced by a 2.4μm interplanetary dust grain entering the detector with
3.4 ± 0.5km/s, from which the dust trajectory (blue line in the left plot) has
been reconstructed.

ticle is approaching the first inner grid ($t_0 \le t < t_1$). As soon as the particle is between
the two inner grids, QP remains at a constant value that is proportional to the dust
charge. Consequently, the dust charge Q_d can be directly derived from the QP signal
averaged over $t_1 \le t < t_2$. After passing grid 2, QP decreases again until the particle
passes the inner shield grid 3 ($t_2 \le t < t_3$).

The inclined mounting of the two inner grids causes an entrance angle-dependent
asymmetric shape of QP. This can be used to obtain additional information about the
grain's velocity vector. Having two inclined grids implies that one can directly determine the velocity vector projected into the y–z–plane, i.e. two independent velocity
components. As Auer (1975) and Auer et al. (2002) pointed out, a design with 4 inclined grids allows one to determine all three velocity components. However, keeping
in mind that instruments on spacecraft face tough weight restrictions, the two-grid design on CDA is a good compromise between achieving a sufficient accuracy and the
desire for a large instrument field-of-view.

The charge signal is continuously sampled at 6 MHz, digitised with 8 bit resolution,
and temporarily stored in a 1372 elements "Last In First Out" memory (LIFO). After
a measurement cycle is triggered by the IID, the LIFO is stopped and read out by the
on-board computer. Again, as for the impact ionisation signals, the QP data may be

Table 1.1.: QP geometrical parameters.

	Value	Description
γ	8.99°	inclination of grid 1 and 2
d_0	16.2 mm	distance between grid 0 and 1
d_1	99.6 mm	distance between grid 1 and 2
d_2	80.3 mm	distance between grid 2 and 3
d	196.1 mm	distance between grid 0 and 3
d_3	48.6 mm	distance between grid 3 and the target's geometrical center
d_4	103.3 mm	distance between target center and target rim
h	410.5 mm	target diameter
h_1	432.0 mm	CDA aperture
R	229.4 mm	target radius
ϕ_{IIT}	126.0°	IIT angular size
ϕ_{CAT}	40.8°	CAT angular size

preprocessed by the flight software before transmission.

To allow for the detection of positively as well as negatively charged particles, the induced charge has to be measured with respect to the mean background signal, which is due mostly to the ambient plasma environment. To compensate for the long scale variations of the ambient plasma, the amplifier baseline was designed as floating. The time constant of the baseline electronics was chosen to be larger than the duration of the monitored QP signal of about 229 μs. It should be noted that the absolute value of the baseline must be smaller than the sensitive range of the amplifier; otherwise the amplifier will be saturated. Thus, the QP detector will not provide useful data within plasma rich environments, e.g., the inner solar system.

The speed components of the entering dust particles within the instrument's y-z-plane are

$$v_z = \frac{d}{t_{03}} \tag{1.1}$$

$$v_y = \frac{d_1}{t_{12}} - v_z, \tag{1.2}$$

where $t_{ij} = t_j - t_i$ and $d_0, \ldots, d_2$ and γ are geometrical parameters given in Tab. 1.1. The particle enters at the detector at distance

$$y_0 = \cot\gamma \left\{ \frac{t_{01}}{t_{12}} d_1 - d_0 \right\} - \frac{t_{01}}{t_{03}} \tag{1.3}$$

to the symmetry axis. Finally, the angle between the trajectory in the y-z plane and the

symmetry axis is

$$\tan\alpha = \cot\gamma\left\{\frac{1}{v_z}\frac{d_1}{d} - 1\right\}. \tag{1.4}$$

It is impossible to fully reconstruct the particle's trajectory in the x-z plane, because this would require 3 inclined grids. However, the x coordinate of the site of impact on the detector's spherical target can be deduced from the impact time. Clearly, the particle hits the target in the y-z plane at $y_4 = y_0 + v_y t_{40}$ and $z_4 = v_z t_{40}$. Because of the spherical shape of the impact target, the coordinates of the site of impact have to fulfill the condition $R^2 = x_4^2 + y_y^2 + (z_4 - d_3 - d)^2$ and thus,

$$x_4 = \pm\sqrt{R^2 - y_4^2 - (z_4 - d_3 - d)^2}. \tag{1.5}$$

The x coordinate of the particle's entry point is constrained by the instrument's aperture, i.e.

$$-\frac{h}{2} \leq x_0 \leq \frac{h}{2}. \tag{1.6}$$

Because x component of the particle's speed vector cannot exceed $(x_4 + \frac{1}{2}h)/t_{04}$, the impact speed can only take values between

$$(v_y^2 + v_z^2)^{\frac{1}{2}} \leq v \leq \left(v_y^2 + v_z^2 + t_{04}^{-2}(x_4 + \frac{1}{2}h)^2\right)^{\frac{1}{2}}. \tag{1.7}$$

The minimum value corresponds to the case that the grain's trajectory is parallel to the detector's y-z plane.

1.1.2. Chemical Analyser - CA

Impacts onto the CAT provide a time-of-flight (TOF) mass spectrum (Fig. 1.4). The TOF mass spectrometer was developed by the University of Kent, UK, and has a flight length of 230 mm (Ratcliff et al., 1995). Positive ions generated on the CAT, which is made of rhodium, are accelerated by the electric field between the CAT (being on a potential U_a of the order of +1 000V) and the grounded grid (CA grid - CAG) 3 mm in front of it, and are then collected by the multiplier (MP) beyond the ion grid. The multiplier signal is sampled at 100 MHz and digitised with 8 bit resolution.

The ion's flight time is a direct measure of its mass m. From laboratory experiments with impact speeds between 2km s^{-1} and 70km s^{-1} and using a variety of grain materials the CA mass resolution[1] was found to range between 20 for light atomic species

---

[1]The mass resolution $m/\Delta m$ of a mass spectrometer is defined as the ratio of the ion mass and the line half width.

such as carbon and oxygen and 40 for heavier atoms such as rhodium (Srama et al., 2004). The mass resolution is sufficient for characterising the elemental composition of the impactor but does not allow an isotopic analysis. The maximum detectable atomic mass is about 7000 amu. To achieve a large sensitive area and keep the instrument design simple, the CA does not use an electrostatic reflector for flight-time focusing, a technique which provides improved resolution of spectral lines and which has been used in high-resolution detectors such as those flown on the Giotto and the Stardust mission (Auer, 2001).

Calibration of the signal from volts to coulombs and hence to ion abundance is performed using the QI channel, making assumptions on both the ion losses to the grid and the degree of ionization of the ions which strike the grid or the multiplier. Calibration onto a mass scale is via the TOF-relation: $t = a\sqrt{m} + t_0$, where a is a "stretch" parameter, related to spectrometer's field strengths and geometry, and t_0 is a zeropoint offset, related to the triggering time of the instrument. In an ideal situation, a and t_0 are constant, and known, and the spectra can be reliably calibrated.

With the CA, in particular t_0 varies from impact to impact, requiring at least two peaks to be identified as due to particular ion species before calibrating onto a mass scale. As the velocity distribution of ions within the initial impact plasma is difficult to determine, and varies between ion species and impact (see Hillier et al. (2006) for a more detailed discussion of this), when calibrating spectra using two peaks the chosen peak maxima have to be assumed to be due to ions with the same energy.

1.2. High Rate Detector HRD

The High Rate Detector HRD is an independent detector of the CDA instrument designed to monitor high impact rates up to $10^4 \, \mathrm{s}^{-1}$ in dust-rich environments where the DA is saturated (Srama et al., 2004). The HRD was designed, built, and tested by the University of Chicago and is mounted piggyback on the front of the CDA main sensor (see Fig. 1.1).

The HRD detects impact of at least micron-sized grains by means of two separate polyvinylidene fluoride (PVDF) foil sensors (sensor M: $50 \, \mathrm{cm}^2$, $28 \mu m$ foil; sensor m: $10 \, \mathrm{cm}^2$, $6 \mu m$ foil; the back surface of both foils were coated with Chemglas Z-306, $40 \mu m$ thick). The PVDF foil consists of a thin film of permanently polarised material. A dust impact on the foil produces rapid local destruction of dipoles, causing a current pulse which can be recorded by the electronics (Fig. 1.6). The released current depends roughly on the grain size and on the impact speed (Simpson and Tuzzolino, 1985). To make use of this dependence, the impact triggers at least one of the 4 counters which are arranged in order of increasing thresholds (Tab. 1.2). The detectors were calibrated with $6\ldots65\mu m$ glass particles at the Munich plasma accelerator facility with impact
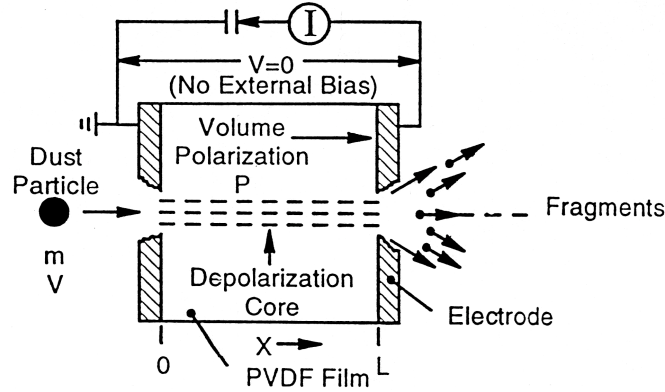
Figure 1.6.: Schematic drawing of a polarised PVDF sample with conduction electrodes. An incident dust particle penetrates the foil resulting in complete depolarisation along its track, causing a fast current pulse. The total released charge is a function of dust mass and speed. From Srama et al. (2004).

counter	charge threshold (#)	grain radius $(v_d = 8\mathrm{km\,s^{-1}})$ (μm)	counter	charge threshold (#)	grain radius $(v_d = 8\mathrm{km\,s^{-1}})$ (μm)
m_1	$2.0{\cdot}10^6$	0.9	M_1	$1.6\cdot10^6$	2.1
m_2	$1.9{\cdot}10^7$	1.6	M_2	$2.8\cdot10^7$	4.2
m_3	$4.1{\cdot}10^8$	3.5	M_3	$6.2\cdot10^8$	8.6
m_4	$5.2{\cdot}10^9$	6.7	M_4	$5.2\cdot10^9$	11.9

Table 1.2.: Impact charge thresholds and corresponding radii of ice particles impacting with $8\ \mathrm{km\,s^{-1}}$.

speeds between $2\mathrm{km\,s^{-1}}$ and $12\mathrm{km\,s^{-1}}$. The number of electrons at the input of the HRD charge amplifiers produced by a dust impact was found to depend on the grain mass m_d and the impact speed v_d as

$$n_m = 3.6 \cdot 10^{18} (m_d[\mathrm{kg}])^{1.3} (v_d[\mathrm{km\,s^{-1}}])^{3.0} \tag{1.8}$$

for the m-detector and

$$n_M = 3.8 \cdot 10^{17} (m_d[\mathrm{kg}])^{1.3} (v_d[\mathrm{km\,s^{-1}}])^{3.0} \tag{1.9}$$

for the M-detector. The lower speed limit for detecting an impact is about $1\mathrm{km\,s^{-1}}$; the detectable mass range is $5{\cdot}10^{-19}$ kg to 10^{-13} kg for impact speeds of $40\mathrm{km\,s^{-1}}$ and 10^{-16} kg to 10^{-10} kg for impact speed $5\mathrm{km\,s^{-1}}$.
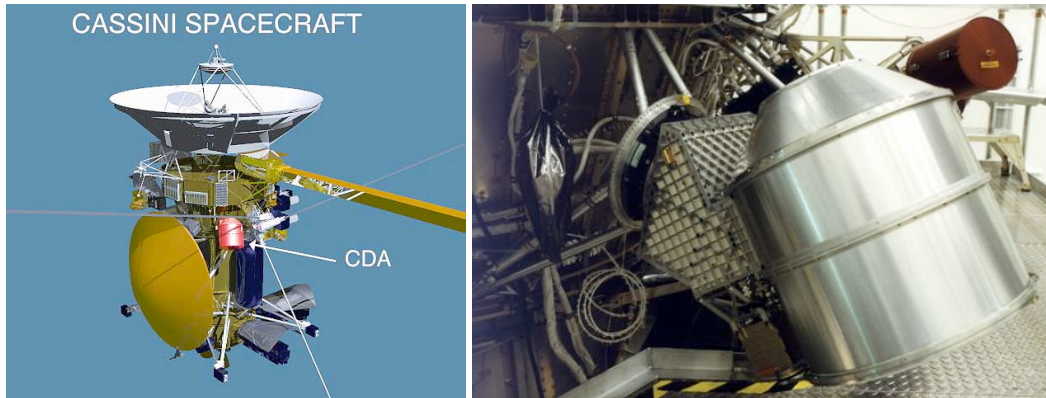
Figure 1.7.: Left: The Cassini/Huygens spacecraft. **Right:** The Cosmic Dust Analyser
mounted at the spacecraft bus.

In Srama et al. (2004) it is claimed that the angular FOV of the HRD is $\pm88°$. In
the inner Saturnian system, however, the HRD did not detect dust grains when the an-
gle between the dust flux and the instrument boresight became larger than about $50°$.
Probably the best explanation for this effect is that oblique impacts on the PVDF foils
do not produce a sufficient amount of impact charges to exceed the lowest threshold
for triggering a measurement. Thus, it is more realistic to assume a HRD FOV of
about $50°$. Note also that the HRD calibration relations 1.8 and 1.9 are valid for small
incidence angles only.

The High Rate Detector is operated by the University of Chicago and its data products
are not discussed in this manual. The HRD team delivers the data as independent
volumes to the PDS.

1.3. Instrument location on spacecraft and CDA field of view

Originally the Cassini-Huygens design included a continuously rotating pointing plat-
form for the fields and particles instruments which was canceled during a descop-
ing process in order to limit the spacecraft costs. Although the CDA instrument was
mounted nearly perpendicular to the Cassini spin axis (Fig. 1.7), wide coverage cannot
be achieved on a mainly 3-axis stabilised spacecraft. Furthermore, the rotation rate
of Cassini is restricted to the maximum value of $0.26°$ s^{-1} and, during high activity
periods, other instruments determine the orientation of the spacecraft. All these con-
straints lead to a redesign of the instrument and a turntable was added at the interface
to the spacecraft.

The mounting vector of the turntable points 15 degrees below the spacecraft x-y plane
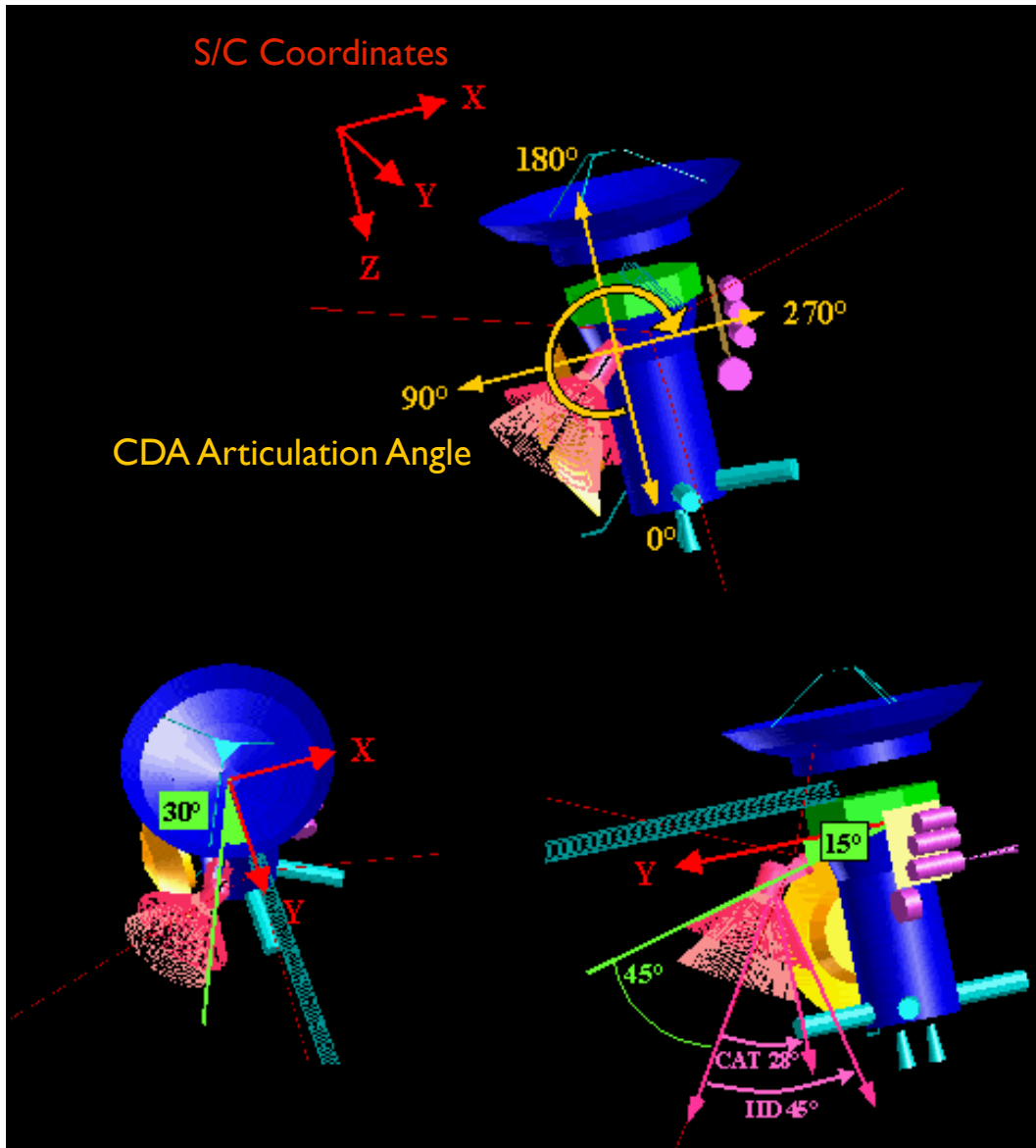
Figure 1.8.: Coordinate system of Cassini and mounting of CDA. The articulation angle of CDA is defined as shown in the top image. The zero degree position of CDA corresponds to the main engine direction. An angle of 90° is compatible with the -X direction which allows combined measurements with the INMS instrument.

(Fig. 1.8). Furthermore, this vector points 30 degrees away from the +y-axis towards -x. The coordinates of the articulation axis with respect to the spacecraft x-y-z coordinate system are (-0.483; 0.837; 0.259). The Dust Analyser detectors (IID, CAT and HRD) are mounted at 45° with respect to the articulation axis. The boresight vector of the field-of-view has the coordinates (-0.250; 0.433; 0.866) in the launch position (0°
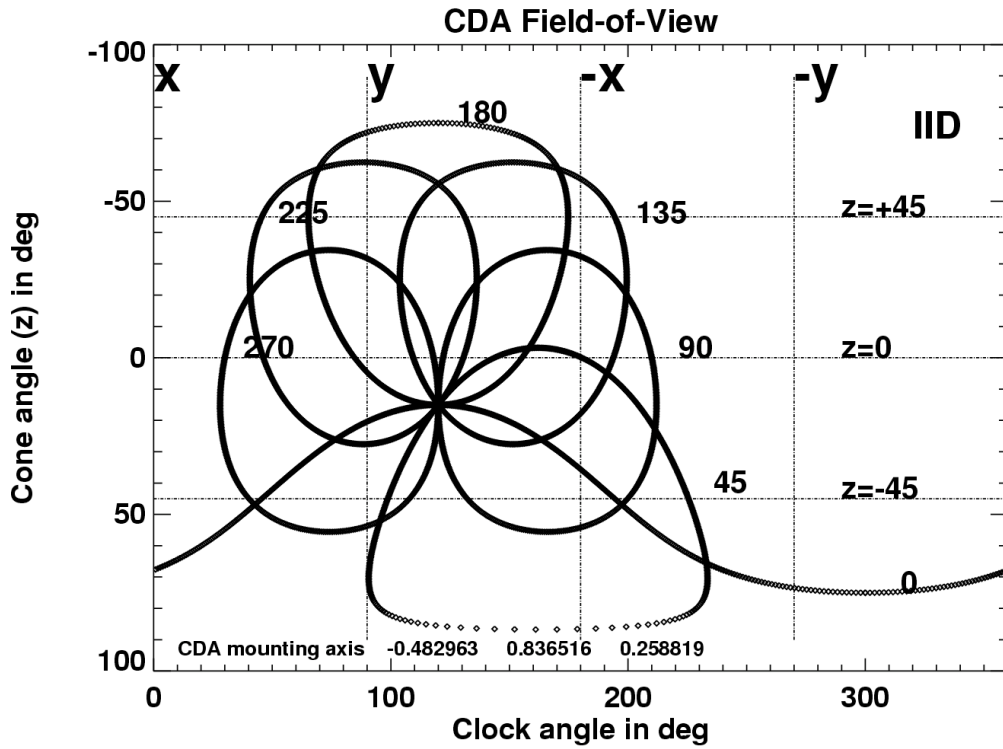
CDA Field-of-View

Figure 1.9.: The field-of-view of the Impact Ionisation Target (IIT) for different articulation angles (0°, 45°, 90°, 135°, 180°, 225° and 270°) in the spacecraft coordinate system. The spacecraft axes are labeled at the top. The z-asymmetry is caused by the mounting of CDA 15° below the x-y-plane. The field-of-view of the CAT is ±28°, while the IID field-of-view is ±45°.

position, downwards to +z). The turntable enables the instrument to rotate by 270°. The cable wrap drum inside the turntable does not allow a full revolution. The lower right quarter of the full circle cannot be reached by the instrument. The spacecraft coordinate system is such that the x-y plane is perpendicular to the spacecraft spin axis z. The +z direction points to the main engine, whereas the Huygens probe points towards -x. Besides the high gain antenna (which points towards- z), Cassini-Huygens has two low gain antennas (LGA). LGA 1 points towards the -z direction whereas LGA 2 points towards the Huygens probe (-x-axis). During Cassini's cruise through the inner Solar system, the 3-axis stabilised spacecraft has an orientation such that the high gain antenna points towards the Sun and the selected low gain antenna points towards the Earth as precisely as possible. Fig. 1.9 shows the field-of-view of the IIT for a variety of articulation angles in the spacecraft coordinate system.

Table 1.3.: CDA event counter scheme (CDA FSW < 10.0). Note that the verbal description of the event type may be misleading.

event counter #	event class #	description	length (bits)
0	1	correctly executed test pulse	8
1	1	incorrectly executed test pulse	8
2	3	impact on CAT, many lines	8
3	3	impact on CAT, few lines	8
4	3	FSW information	8
5	3	noise: high base line	8
6	3	strong, fast impact on IID	8
7	3	strong, slow impact on IID	8
8	3	strong, fast impact on CAT	8
9	2	strong, slow impact on CAT	8
10	2	fast impact on IID	16
11	2	slow impact on IID	16
12	2	fast impact on CAT	16
13	2	slow impact on CAT	16
14	2	strong impact on IID, relaxed requirements	16
15	2	strong impact on CAT, relaxed requirements	16
16	0	noise event: "QI flare"	16
17	0	noise event: may be very faint CAT impact	16
18	0	noise event: may be very faint IID impact	16
19	0	noise event: everything else	16

1.4. Onboard data processing

The CDA measurements are controlled by the instrument's onboard 6 MHz MA31750 microprocessor system, which continuously compares the signals of the 5 amplifiers with channel-specific reference values. If one threshold is exceeded, an event trigger is released. After an event trigger occurred, the sampling frequencies for the QC, QT, and QI channels and the DLA are increased and the signals are digitised and stored in memory. Then, the computer calculates the signal rise times, amplitudes and integrals. A wavelet algorithm allows signal smoothing and a lossy compression. Furthermore, a lossless RICE compression algorithm can be employed to reduce the volume of the raw data by a factor of three. The calculated signal parameters are used further for the onboard data classification. Each event increases the value of one of twenty (FSW $\leq$ 10.0) or twenty six (FSW > 10.0) counter values (see Sec. 1.4.1). About half of the instrument memory is needed for the execution of the onboard software. The remaining memory is used to store event data.

Table 1.4.: CDA event counter scheme (CDA FSW ≥ 10.0). Note that the verbal description of the event type may be misleading.

name	event counter #	event class #	description	length (bits)
A0	0	3	strong impact on CAT, many lines	8
A1	1	3	impact on CAT, many lines	8
A2	2	3	strong impact on CAT, some lines	8
A3	3	3	impact on CAT, some lines	8
A4	4	3	faint impact on CAT, some lines	8
A5	5	2	very faint impact on CAT, some lines	8
A6	6	2	faint impact on CAT, no lines	8
A7	7	2	impact on CAT, relaxed ?	8
A8	16	2	very faint impact on CAT	12
I0	8	3	very strong impact on IID	8
I1	9	3	strong and fast impact on IID	8
I2	10	3	fast impact on IID	8
I3	17	2	faint and fast impact on IID	12
I4	11	3	strong and slow impact on IID	8
I5	12	3	slow impact on IID	8
I6	18	2	faint and slow impact on IID	12
I7	19	2	very faint impact on IID	12
W0	20	0	strong impact on the wall	12
W1	21	0	impact on the wall	12
B0	13	0	faint impact on either CAT or IID	8
N0	22	1	noise event: high signal baseline	12
N1	14	1	noise event: "QI flare"	8
N2	23	0	noise event: everything else	12
T0	24	1	CDA test pulse, correctly executed	4
T1	25	1	CDA test pulse, incorrectly executed	4
E0	26	0	FSW monitoring	8
S0	15	0	spare counter	8

The signals of the channels QP, QC, QT, QI and MP are digitized with 8 bit resolution and are stored in a raw data frame. To save power the channels QC, QT and QI are sampled with 0.375 MHz until an event is detected. After the trigger, the sampling frequencies are increased to 6 MHz (QC and QI) and 3 MHz (QT), respectively. The last 16 samples preceding the trigger are stored together with the nominally sampled data points. The processing of the event data takes one second and is enforced by the onboard software. The major software processing steps are:

1. Buffer read-out of channels QC, QP, QI, QT, DLA

2. Integer wavelet transformation of the recorded signals

3. Set small coefficients to zero (leads to a smooth curve after reverse transformation)

4. Reverse transformation with most significant coefficients

5. Determination of peaks, rise times, amplitudes and times at 50% of the full signal amplitude

6. Classification of the event and increment the appropriate counter

7. RICE compression of the already wavelet-transformed data

8. Activate the event trigger

1.4.1. Event classification

The classification and priorisation of the onboard data is essential for an optimal and effective data transmission. Based on a robust set of criteria, the software associates each event with an "event type". The scheme used until CDA software version 10.0 distinguished 20 event types (Tab.1.3) and was based on the experience of the Galileo dust detector team and on the calibration experiments with the CDA flight spare unit in the Heidelberg dust accelerator. However, the characteristics of ice particle impacts turned out to be not well matched by this scheme. Therefore, later flight software versions employ a more intuitive 26 event type scheme (Tab.1.4). However, it is important to note that the verbal descriptions of the event types are often misleading and should not be taken too seriously. Eventually this is because of the large variability of the signals caused by similar impacts. The event counters are grouped into 4 event classes:

class 0: noise events

class 1: test pulses

class 2: likely impact candidates

class 3: "clearly" identified impacts.

It cannot be stressed enough that the assigned event class is not a reliable indicator for the true nature of a registered event. The computational power of the CDA onboard computer is just not sufficient to identify reliably faint or uncharacteristic dust impacts. As an example, the majority of Jovian and Saturnian stream particle impacts were identified by the flight software as noise events (Kempf et al., 2005; Postberg et al., 2006). Despite of the limitations of the classification scheme, the event class is the main criterion for the FSW for selecting the scientifically most relevant subset of the recorded events for transmission to Earth.

Usually the available data rates are insufficient to transmit the complete raw data sets to Earth. Because such limitation are expected, the CDA flight software stores the total number of the registered event types internally and additionally transmits snapshots of the counting states every 30 seconds to Earth.

1.5. Transmitted CDA data

The onboard software delivers the following data types to the Cassini data system for further transmission to Earth:

- DA raw signals and event parameters including the impact ionization signals, the multiplier signal MP and the charge detector signal QP

- the event counter snapshots

- the CDA housekeeping data

- the High Rate Detector data

There are actually various possibilities, how and in which combination these data products are transmitted. For the data user this is of no relevance because the CDA ground segment repackages the received data accordingly.

1.6. Processing CDA data

The Cosmic Dust Analyser is the most complex and versatile dust detector employed on a spacecraft so far.Naturally, the CDA data are complex as well and there are many ways to analyze a data set. In most cases a user wants to determine the flux of cosmic dust with a specific property (e.g. larger than a given mass, being a E ring particle, or being composed of water ice) throughout a time interval.

1.6.1. Processing steps to derive the dust flux

The derivation of the flux involves typically the following processing steps:

1. Identify noise events amongst the events transmitted during the time of interest (see 3.1.1)

2. Identify which region of the hemispherical target (IIT or CAT) did the particles hit (see Sec. 3.1.2), because the calibration relations for IIT and CAT impacts are different (see Sec. 3.2 and 3.3)

3. Derive the mass and impact speed for the impact events (see Sec. 3.2 and 3.3)

4. Determine for CAT impacts the composition of the registered dust grains

5. Determine, if possible, the origin of the dust grains (e.g. from the impact parameters)

6. Correct the data set for incomplete data transmissions by correlating the transmitted data with the event counter data set (see Sec. 4.1)

7. Correct the dust impact rate for instrument dead time effects (see Sec. 4.2)

8. Determine the effective sensitive area to transform the impact rate into the dust flux (see Sec. 4.3)

In some cases, these steps may not be sufficient and a more extensive data analysis involving auxiliary data is unavoidable (e.g. Kempf et al. (2008)).

1.6.2. CDA data products to derive the dust flux

To derive the dust flux registered by CDA the user needs to have at least the following data products:

1. the characteristic impact ionization parameters of the individual events

2. the event counter data recorded by CDA during the time of question

3. spacecraft ephemerides (SPICE SPK) and orientation (SPICE CK) data for the time of interest

4. CDA position data (CDA articulation file) for the time of interest

2. CDA Data Access

2.1. Types of Instrument Data available at the PDS Node

2.1.1. CDA Data Processing Levels

The CDA processed data uses the Committee On Data Management And Computation (CODMAC) data level numbering system. The scientist will likely begin using level 2 or Edited Data (equivalent to NASA level 0). The data files are generated from level 1 or Raw Data which is the telemetry packets within the project specific Standard Formatted Data Unit (SFDU) record. Please refer to the next Table.

NASA	CODMAC	Description
Packet data	Raw - Level 1	Telemetry data stream as received at the ground station, with science and engineering data embedded.
Level 0	Edited - Level 2	Instrument science data (e.g., raw voltages, counts) at full resolution, time ordered, with duplicates and transmission errors removed.
Level 1-A	Calibrated - Level 3	Level 0 data that have been located in space and may have been transformed (e.g., calibrated, rearranged) in a reversible manner and packaged with needed ancillary and auxiliary data(e.g., radiances with the calibration equations applied).
Level 1-B	Resampled - Level 4	Irreversibly transformed (e.g., resampled, remapped, calibrated) values of the instrument measurements (e.g., radiances, magnetic field strength).
Level 1-C	Derived - Level 5	Level 1A or 1B data that have been resampled and mapped onto uniform space-time grids. The data are calibrated (i.e., radiometrically corrected) and may have additional corrections applied (e.g., terrain correction).

Table 2.1.: Processing Levels for Science Data Sets

NASA	CODMAC	Description
Level 2	Derived - Level 5	Geophysical parameters, generally derived from Level 1 data, and located in space and time commensurate with instrument location, pointing, and sampling.
Level 3	Derived - Level 5	Geophysical parameters mapped onto uniform space-time grids.

Table 2.1.: Processing Levels for Science Data Sets

Right now, only NASA Level 0 and 1 data products are delivered to the PDS.

2.1.2. CDA PDS data products

Product Name	Product ID	Description	Subsystem source
CDA Pointing History	CDA-PNT	J2000 Pointing vector of instrument as a function of time when CDA is on	
CDA Area Table	CDA-CAL-AREA	The sensitive area of the CDA impact detector (IID) and chemical analyser (CAT) is tabulated as a function of the incident angle with respect to the instrument axis.	Calib.
CDA Status History	CDA-STAT	Cassini mission and CDA configuration, tests and other events. Records are triggered by change in status affecting the sensitivity of the different CDA instruments and mission events that may affect the interpretation of the data.	SC / DA / HRD
Dust Analyser Impacts Table	CDA_DA_IMPACTS	Detector responses and derived quantities from the Cassini dust detector as well as spacecraft geometry information for reliable impacts.	DA
CDA Spectra Table	CDA-SPECTRA	Time-of-flight mass spectra peaks for individual impact events.	MA
Individual Mass Spectra	MS-XXXXXXX	Time-of-flight mass spectra for individual impacts, identified by their unique identifier number xxxxxx	MA

Product Name	Product ID	Description	Sub-system source
CDA QI Signal Table	QI-XXXXXXX	Ion signals for individual impacts, identified by their unique identifier number xxxxxxx	IID
CDA QT Signal Table	QT-XXXXXXX	Electron signals for individual impacts, identified by their unique identifier number xxxxxxx	IID
CDA QC Signal Table	QC-XXXXXXX	Electron signals for individual impacts, identified by their unique identifier number xxxxxxx	IID
CDA QP Signal Table	QP-XXXXXXX	Induced charge signal for individual impacts, identified by their unique identifier number xxxxxxx	IID
CDA Settings Table	CDA-CAL-SET	Table of voltages corresponding to voltage level codes and Coulomb threshold settings.	Calib.
CDA Counter Table	CDA-DA-CTR	CDA impact counter time history file.	DA

2.1.3. Data Unit Definition

The CDA data products delivered to the PDS are already converted into physical units such as Coulomb or Volt.

2.2. List of tools in the PDS used for data calibration

CDA hasn't delivered any dedicated data processing tools to the PDS yet.

2.3. List of tools outside the PDS

There are some standard tools useful for reading, processing, and analyzing CDA data:

- Internet software capable of performing FTP, SFTP functions, in order to download CDA PDS archive sets and the NAIF library.

- https://naif.jpl.nasa.gov/pub/naif/pds/data/co-s_j_e_v-spice-6-v1.0/cosp_1000/
  for extracting spacecraft and instrument ephemeris infor-mation. The library
  can be integrated with your programming language of choice: C, Fortran,
  IDL, Matlab.

- Programming language of choice such us C, Fortran, IDL, or Matlab.

- IDL routine(s) to read a PDS archive, or write your own. We used:readPDS
  (https://pdssbn.astro.umd.edu/tools/tools_readPDS.shtml).

We developed a small IDL software package for a quick-look analysis of the CDA
PDS data, which is included in the Appendix E.

2.4. How to search the instrument data In the PDS

2.4.1. Introduction

Assume we have chosen Orbit 3, which contains the Enceladus encounter in 2005 on
day 48. That would be a part of the following dataset (see Appendix C):

```
COCDA_0007 2005-001 2005-090 331 MBytes COCDA_0007.tar.gz
```

The data directory for that particular CDA dataset will look similar to the following:

```
10 % dir
total 56
drwxr-xr-x 9 amaragra amaragra 306 Aug 26 2010 .
drwxr-xr-x 4 amaragra amaragra 136 Sep 6 08:44 ..
-rw-r--r-- 1 amaragra amaragra 1720 Dec 19 2005 AAREADME.TXT
drwxr-xr-x 10 amaragra amaragra 340 Dec 27 2005 CATALOG
drwxr-xr-x 20 amaragra amaragra 680 Dec 19 2005 DATA
drwxr-xr-x 7 amaragra amaragra 238 Dec 27 2005 DOCUMENT
-rw-r--r-- 1 amaragra amaragra 1360 Dec 19 2005 ERRATA.TXT
drwxr-xr-x 7 amaragra amaragra 238 Dec 19 2005 INDEX
-rw-r--r-- 1 amaragra amaragra 3411 Aug 26 2010 VOLDESC.CAT
```

with the required PDS archive files and directories, described by **CDA_SIS_1.2.DOC**.

`AAREADME.TXT` file that contains an overview of the contents and structure of the
volume, in which we see the rest of the contents of a typical CDA archive described in
an abbreviated form:

```
* FILE                  CONTENTS
Top-level directory
```

```
|
|- AAREADME.TXT        The File you are reading
|
|- ERRATA.TXT          Description of known anomalies and errors
|                      present on this volume.
|
|- VOLDESC.CAT         A description of the contents of this volume
|
|[CATALOG]             A directory containing the catalog
| |                    files with information about the
| |                    CDA dataset, instrument, and mission.
| |
| |-MISSION.CAT        Mission catalog file
| |-INSTHOST.CAT       Instrument host (spacecraft) catalog file
| |-CDAINST.CAT        CDA instrument catalog file
| |-CDADS.CAT          CDA data set catalog file
| |-CDAREFS.CAT        Reference list catalog file
| |-PROJREF.CAT        Project reference list catalog file
| |-DUST.CAT           Target catalog file
| |-CATINFO.TXT        Description of files in the CATALOG directory
|
|[INDEX]               A directory containing index files for this volum
| |
| |-INDEX.TAB          Index of the contents of this volume
| |-INDEX.LBL          Detached label for index
| |-CUMINDEX.TAB       Index of all volumes published to date
| |-CUMINDEX.LBL       Detached label for cumulative index
| |-INDXINFO.TXT       Description of files in the INDEX directory
|
|[DATA]                Directory containing the data products
| |
| |-DATAINFO.TXT       Description of files in the DATA directory
|
| |-CDAAREA.LBL        PDS label object.  Description of
| |                    CDA sensitive area data.
| |
| |-CDAAREA.TAB        PDS table object.  Sensitive area data.
| |
| |-CDACOUNTER.LBL     PDS label object.  Description of
| |                    CDA counter state data.
| |-CDACOUNTER.TAB     PDS table object.  Counter state data.
| |
| |-CDAEVENT.LBL       PDS label object.  Description of
```

```
| |                        CDA event data.
| |-CDAEVENT.TAB       PDS table object.  Event evaluation data.
| |
| |-CDAPOINTING.LBL    PDS label object.  Description of
| |                    CDA pointing data.
| |-CDAPOINTING.TAB    PDS table object.  Pointing data.
| |
| |-CDASETTINGS.LBL    PDS label object.  Description of
| |                    CDA settings data.
| |-CDASETTINGS.TAB    PDS table object.  Settings data.
| |
| |-CDASPECTRA.LBL     PDS label object.  Description of
| |                    CDA TOF mass spectra data.
| |-CDASPECTRA.TAB     PDS table object.  TOF mass spectra data.
| |
| |-CDASTAT.LBL        PDS label object.  Description of
| |                    CDA status data.
| |-CDASTAT.TAB        PDS table object.  CDA status data.
| |
| |-[QISIGNALS]        Directory containing individual
| | |                  impact signals
| | |                  XXXXXXX represents the id of each signal.
| | |-QI_XXXXXXX.LBL PDS label object.  Description
| | |                  of QI signal data.
| | |-QI_XXXXXXX.TAB PDS table object.  QI signal data.
| | |
| |-[QTSIGNALS]        Directory containing individual
| | |                  impact signals
| | |-QT_XXXXXXX.LBL PDS label object.  Description
| | |                  of QT signal data.
| | |-QT_XXXXXXX.TAB PDS table object.  QT signal data.
| | |
| |-[QCSIGNALS]        Directory containing individual
| | |                  impact signals
| | |-QC_XXXXXXX.LBL PDS label object.  Description
| | |                  of QC signal data.
| | |-QC_XXXXXXX.TAB PDS table object.  QC signal data.
| | |
| |-[QPSIGNALS]        Directory containing individual
| | |                  impact signals
| | |-QP_XXXXXXX.LBL PDS label object.  Description
| | |                  of QP signal data.
| | |-QP_XXXXXXX.TAB PDS table object.  QP signal data.
```

2. CDA Data Access

```
| | |
| |-[MPSIGNALS]        Directory containing individual
| | |                 impact signals
| | |-MP_XXXXXXXX.LBL PDS label object.  Description
| |                   of MP signal data.
| | |-MP_XXXXXXXX.TAB PDS table object.  MP signal data.
|
|
|-[DOCUMENT]           Directory containing supporting documents
|
|-Software Interface Specification (SIS)
|-DOCINFO.TXT          Description of files in the DOCUMENT directory
```

In this PDS CDA Archive, `COCDA\_0007,` we see in DATA the following files and directories:
```
      7520   Dec 14 2005  CDAAREA.LBL
      1274   Dec 14 2005  CDAAREA.TAB
     22880   Dec 14 2005  CDACOUNTER_05001_05090.LBL
   5830400   Dec 14 2005  CDACOUNTER_05001_05090.TAB
     44080   Dec 14 2005  CDAEVENTS_05001_05090.LBL
  14599424   Dec 14 2005  CDAEVENTS_05001_05090.TAB
     19120   Dec 15 2005  CDASETTINGS.LBL
     21504   Dec 15 2005  CDASETTINGS.TAB
       602   Dec 19 2005  CDASPECTRA_00001_00090.TAB
     68240   Dec 19 2005  CDASPECTRA_05001_05090.LBL
     23760   Dec 14 2005  CDASTAT_05001_05090.LBL
     23110   Dec 14 2005  CDASTAT_05001_05090.TAB
      1520   Dec 19 2005  DATAINFO.TXT
   3053370    Jul 8 2009  MPSIGNALS_05001_05090
   3053370    Jul 8 2009  QCSIGNALS_05001_05090
   3053404  Sep 13 06:35  QISIGNALS_05001_05090
   3053370    Jul 8 2009  QPSIGNALS_05001_05090
   3053370    Jul 8 2009  QTSIGNALS_05001_05090
```
where the pointing information table

```
| |-CDAPOINTING.LBL   PDS label object.  Description of
| |                   CDA pointing data.
| |-CDAPOINTING.TAB   PDS table object.  Pointing data.
| |
```

is missing. This is because the orientation of the CDA boresight given in the inertial J2000 frame is given for each impact event in the PDS table CDA_DA_IMPACTS (column 32: DETECTOR RIGHT ASCENSION and column 33: DETECTOR DECLINATION).

2.4.2. Search methods to produce complete data set

Types of searches

CDA is a survey instrument and does not perform target-sensitive observations. In almost all cases the only reasonable search strategy is to identify all data acquired during a time interval and to analyze the resulting data set.

Search and navigation strategies when interfacing with the PDS index file and SPICE

NAIF SPICE provides the necessary functionality to identify CDA observation periods during which the instrument was for instance sensitive to a certain dust family. The SPICE kernels for the Cassini mission are archived in the PDS. There is a comprehensive set of SPICE tutorials available. Once the time period is known the corresponding data set is built up by scanning the CDA_DA_IMPACTS table for events registered during the period of interest. The end-to-end example in Section 2.5.1 explains in detail how a such a data set is compiled.

Keywords to find specfic data

CDA hasn't delivered yet high level data products such as dust composition types or the grain origin to the PDS. Thus, there is no "specific" property for which the CDA PDS volumes can be searched.

2.5. End-to-end example

The work of interest to reproduce spectra in that of Postberg et al. (2008). The parameters of Cassinis crossings through Saturns ring plane considered for this work appears in Table 2 of the companion paper by Kempf et al. (2008). The UTC time tag in the Table 2 is given in the format: DOY:hh:mm, where DOY is day-of-year, hh = hour, and mm = min. In order to determine the date in which to extract the data, the spacecraft event time SCET for the target encounter, Enceladus, will be used, with the DOY from the next table column providing supplementary information. For example, in Orbit 3 Cassini crossed Saturn's ring plane on February 17, 2005, DOY 48, at 03:24 UTC.

The main figures in the Postberg et al. (2008) paper to reproduce are Figures 2a and 2b, which show typical examples of E-ring water ice spectra (Fig. 2.1). The spectra have been recorded at 2005-177T13:39:28 and 2005-177T21:25:14, respectively, which was during the ring plane crossing in orbit 10. According to Table C.1, this data is part of the COCDA_0011 PDS delivery.
All labelled peaks are due to ions formed from water molecules. The mass in atomic mass units (amu) is labelled below the molecular species. The hydronium ion H_3O^+
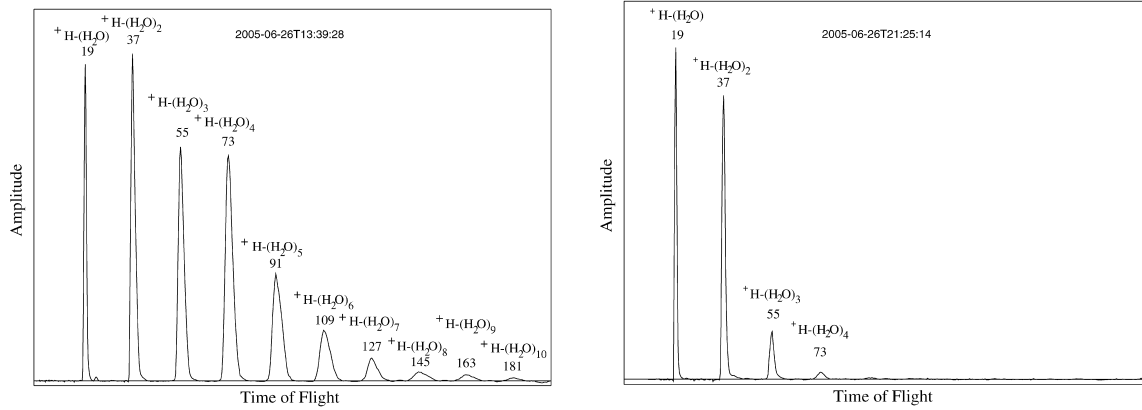
Figure 2.1.: Figures 2a and 2b from Postberg et al. (2008), which will be reproduced in this end-to-end example.

with a mass of 19 amu is followed by a sequence of cluster ions of the form $(H2O)_xH^+$ with 18 amu gaps in between. Both impacts have similar total ion yields and amplitudes. Different impact conditions lead to a different appearance of water clusters - e.g. high energy densities preferably lead to short clusters. The spectrum amplitude has been slightly smoothed. The CDA Multiplier signal MP constitutes the time-of-flight mass spectrum of the impact plasma generated by the dust particle impact (see Section 1.1.2). Thus, to reproduce the results of the Postberg et al. (2008) paper the user needs to find and analyze the CDA MP signals contained in the CDA PDS volume COCDA_0011.

The analysis of the Postberg et al. (2008) paper is based on CDA mass spectra obtained during the Cassini ring plane crossings 3, 4, 7, 8, 9, 10, 11 and 20. The crossing duration was assumed to be ±30 minutes around the ring crossing times given in Kempf et al. (2008). The initial dataset is based on all transmitted data identified as impacts on the CAT (see Section 3.1.2). From this data set, only spectra of a compression factor 2 or less with at least two distinct mass lines were selected. The information about the impact site is given in the CDA PDS table CDA_DA_IMPACTS (column 15: TARGET FLAG), while the compression factor of the mass spectrum in question is given in the CDA PDS table CDA-STAT (column 18: MP SHRINKING).

2.5.1. Step by step instructions for gathering complete dataset

- From the PDS Archive:https://sbn.psi.edu/pds/`pds/`
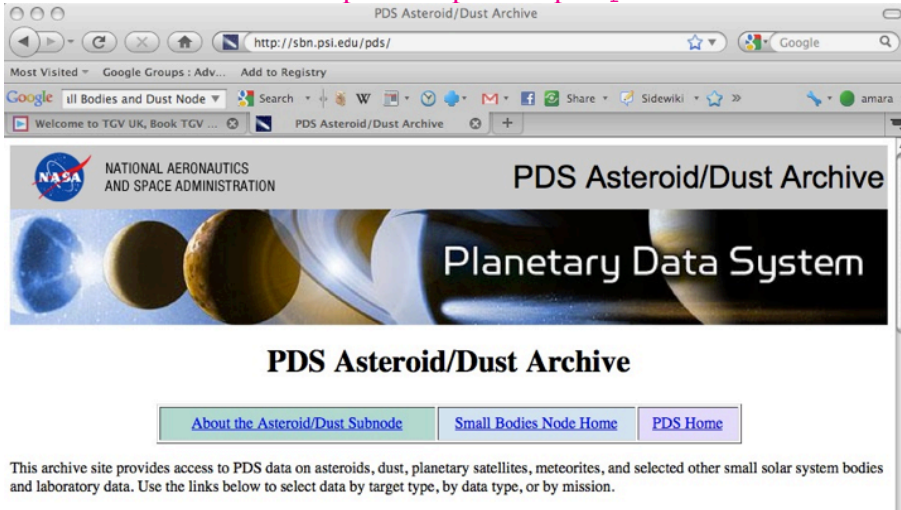
- Click on **All Dust Data**

- Select data by mission: Cassini Cosmic Dust Analyzer (CDA)

-

- Once one has the orbit and a UTC time for the data of interest, one can note the year and any other general timing information from the file stored in the PDS.

- Download the desired data by clicking on the file containing the time period of interest and save it to your desired location on your computer. The data are stored in gzipped and tared files. For example, Orbit 10, which contains the ring plane crossing at day 2005-177, would be a part of the dataset COCDA_0011.tar.gz

- gunzip the file:
  `gunzip COCDA_0011.tar.gz`

- tar-extract it:
  `tar -xvf COCDA_0011.tar`

- Load the table `CDAEVENTS\_05001\_05090.TAB,` which is of the object type CDA_DA_IMPACT and is stored in the `DATA` directory, into your preferred data processing software such as IDL. Here we use the IDL package pds_read_table.pro, which can be found in the appendix of this document:

```
ev = pds_read_table('DATA/CDAEVENTS_05091_05181.LBL')
```

2. CDA Data Access

Now, the structure array `ev` contains the content of the events table, where the structure tag names correspond to the names of the PDS table columns.

- Compute the Julian Day start and end time of the period in question (using e.g. the IDL function JULDAY) and identify all events (i.e. rows), which event time lies within the desired time range. As an example, the the list of events registered by CDA ±30 minutes around the ring plane crossing in orbit 10 can be obtained by the following procedure:

```
jd0 = pds_utc2jd('2005-177T13:29:00') - 30.D/1440.D
jd0 = pds_utc2jd('2005-177T13:29:00') + 30.D/1440.D
iSet = WHERE(ev.EVENT_JULIAN_DATE GE jd0 AND     $
             ev.EVENT_JULIAN_DATE LE jd1, nSet),
```

resulting in a list of 357 events. To compile a data set, which only includes CAT impacts ("mass spectra"), do:

```
jd0 = pds_utc2jd('2005-177T13:29:00') - 30.D/1440.D
jd0 = pds_utc2jd('2005-177T13:29:00') + 30.D/1440.D
iSet = WHERE(ev.EVENT_JULIAN_DATE GE jd0 AND     $
             ev.EVENT_JULIAN_DATE LE jd1 AND $
             ev.TARGET_FLAG EQ 9, nSet)
```

which results in an empty data set. It turns out that the calibration of the data was not finished at the time of the PDS delivery (indicated by the fact that the TARGET FLAG column of all events is set to the "missing data" value 9.
The CDA events corresponding with the 2 spectra in the Postberg et al. (2008) paper are found by doing:

```
dt = 0.5D/86400D ;; 0.5 seconds in JD
iSpec1 = WHERE(ABS(ev.EVENT_JULIAN_DATE - $
               pds_UTC2JD('2005-177T13:39:28')) LT dt)
iSpec2 = WHERE(ABS(ev.EVENT_JULIAN_DATE EQ $
               pds_UTC2JD('2005-177T21:25:14')) LT dt)
```

- Compile a list of the `IMPACT EVENT` IDs of those events:

```
id = ev[iSet].IMPACT_EVENT_ID
```

The IDs of the 2 spectra in the Postberg et al. (2008) paper are obtained by:

```
idSpec1 = ev[iSpec1]
idSpec2 = ev[iSpec2]
```

The IDs are found to be 368774 and 370056.

- Load the multiplier signal tables (Product ID MP-XXXXXXX) for the selected events from the DATA/MPSIGNALS_MPSIGNALS_05091_05181. There is one MP signal table for each event. The table name is composed of the prefix MPSIGNAL_S_ and the IMPACT EVENT ID. To read in the MP signals of the 2 spectra do:

```
mp1 = 'DATA/ MPSIGNALS_05091_05181/MP_' + $
      STRING( idSpec1 , FORMAT = '( I08 ) ') + '.LBL'
mp2 = 'DATA/ MPSIGNALS_05091_05181/MP_' + $
      STRING( idSpec2 , FORMAT = '( I08 ) ') + '.LBL'
spec1 =  pds_read_table(mp1)
spec2 =  pds_read_table(mp2)
```

- The second column of a MP-XXXXXXX table contains the ion flight times relative to the event trigger time and the second column is the MP amplitude in V. Now, the time-of-flight spectrum is available for further analysis by the user. As an example to plot the first spectrum of the Postberg et al. (2008) paper do:

```
PLOT,  spec1.offset_time ,  spec1.amplitude ,  XRANGE =  [0.,  6.0]
```

resulting in
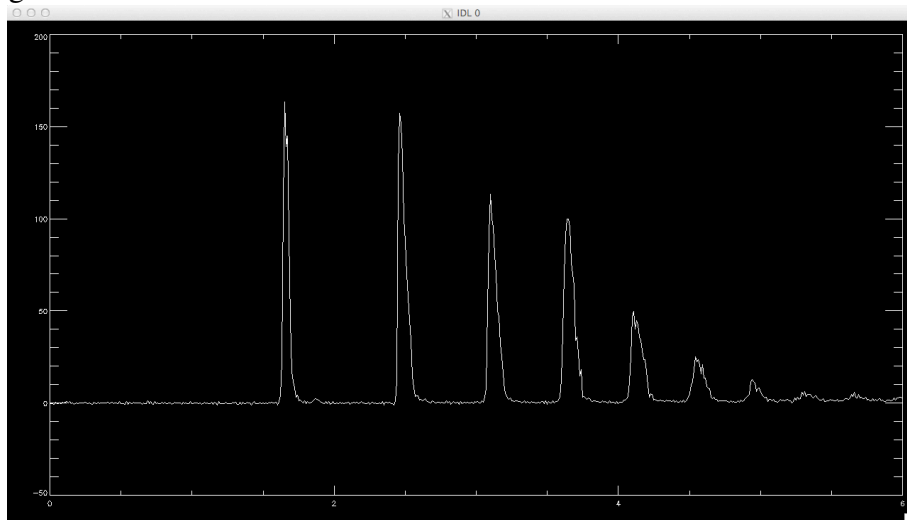
Note that the spectra amplitudes in the Postberg et al. (2008) paper are plotted logarithmically.

2.6. List of key problems and troubleshooting methods

- CDA PDS tables sometimes have invalid entries. These problems should be fixed when updated data products are redelivered to the PDS.

- The current design of the CDA PDS data structure leads to a very large number of tables (easily around a million tables per volume). This not only causes very long computer times for untaring the volumes but also too ineffective data handling. The design of the waveform tables should be changed to PDS stream objects.

- The CDA SIS 1.2 does not reflect exactly the current architecture of the data volumes.

3. Mass and speed calibration of individual dust impacts

3.1. Identification of the dust impact site

3.1.1. Criteria for a genuine dust impact

A measurement is often triggered by effects not associated with a dust impact. Through extensive calibration experiments with the CDA flight spare unit in the Heidelberg dust accelerator, the following criteria for identifying genuine impacts were established:

- Since an impact plasma is electrically neutral, a dust impact must be accompanied by at least one target signal ($q_{QC} > 0$ or $q_{QT} > 0$) and an ion grid signal ($q_{QI} > 0$). Note that the later criterion does not imply a non-zero multiplier signal, i.e. $U^{(MP)} \geq 0$.

- The efficiency of collecting ions at the ion grid is generally smaller than the efficiency of collecting electrons at the impact target, i.e. $q_{QC} + q_{QT} \approx 3 \ldots 20\, q_{QI}$.

- Electrons are collected at their point of origin while the plasma ions have to move to the ion grid (distance 229 mm). Therefore, the maximum amplitude of at least one of the target signals has to be established before the maximum of the ion grid signal, i.e. $\min(t_{100\%}^{(QC)}, t_{100\%}^{(QT)}) < t_{100\%}^{(QI)}$.

- Plasma ions escaping the instrument frequently cause very strong positive QP signals after the trigger instant. Thus, $\min(t_{100\%}^{(QC)}, t_{100\%}^{(QT)}) < t(\max(QP))$ is a useful indicator for an impact on the DA target. On the other hand, a strong rise of the QP before the trigger instant is caused by impacts onto one of the QP entrance grids.

- A clear TOF line spectrum indicates a dust impact on the CAT

(Kempf et al., 2004).

3.1.2. Identification of the impact site

Due to the accelerator grid in front of the inner target, impacts onto the CAT cause signals different from those generated by IIT impacts. Furthermore, the calibration

Figure 3.1.: Numerical simulation of the propagation of electrons and positively charged ions for an impact on the CAT. Left: propagation of 30 eV plasma electrons; Middle: propagtion of 3 eV ions; Right: propagation of 30 eV ions. Note that most of the positive plasma ions are collected at either the ion grid or the multiplier. From Grün et al. (2002).

Figure 3.2.: Numerical simulation of the propagation of electrons and positively charged ions for an impact onto the IIT. Left: propagation of 30 eV plasma electrons; Middle: propagtion of 3 eV ions; Right: propagation of 30 eV ions. Note that the efficiency of collecting plasma ions at either the ion grid or the multiplier is much less than for an impact on the CAT. From Grün et al. (2002).

relations are not applicable for impacts onto the instrument walls or onto the entrance grids. Thus, the identification of the impact location is crucial for estimating the mass and speed of the impactor reliably. This is achieved by two methods: one approach is to relate the flight data to calibration measurements performed with the dust accelerator in Heidelberg (Göller and Grün, 1989; Srama, 2000; Stübig, 2002; Srama, 2010). Another powerful way to investigate the instrument response onto the impact location is to simulate numerically the propagation of the plasma constituents within the instrument. Grün et al. (2002) studied the propagation of typical plasma constituents using the SIMION software package, which allows one to model complex field geometries (see Fig. 3.1-3.3).

Based on the results of these two methods the dependence of the impact signals on the impact location can be characterised as follows: regardless of the impact location,
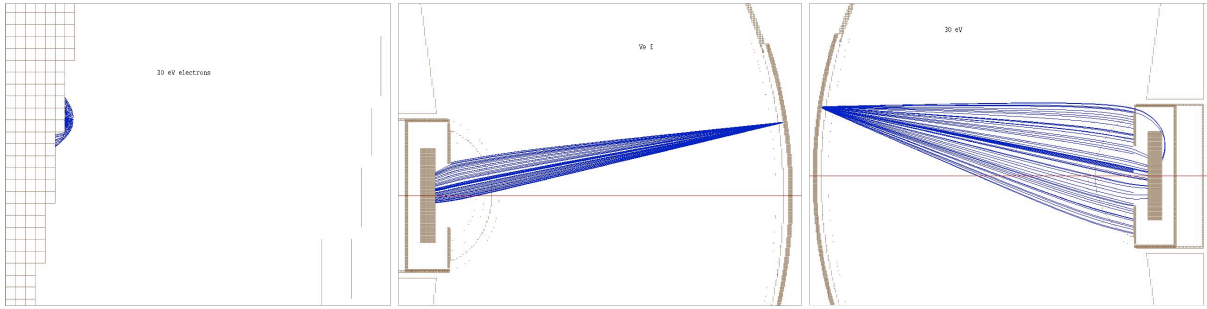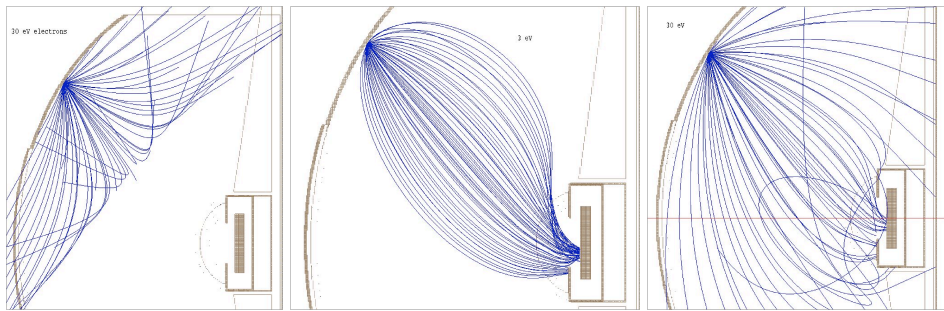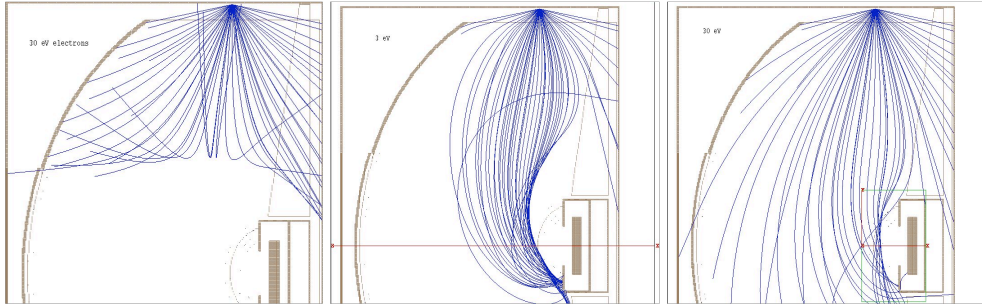
Figure 3.3.: Numerical simulation of the propagation of electrons and positively charged ions for an impact onto the inner wall of the instrument. Left: propagation of 30 eV plasma electrons; Middle: propagation of 3 eV ions; Right: propagation of 30 eV ions. Note that the efficiency of collecting plasma electrons and ions is much less than for target impacts. From Grün et al. (2002).

the DA signals rise as long as charges are available. After that, the amplifiers start to discharge, and thus their amplitudes decline as $\sim \exp(-t/\tau)$, with τ being the time constant of the respective amplifier.

The amplitude measured at the target hit by the particle (IIT or CAT) is usually significantly larger than the complementary target signal. Due to the acceleration grid in front of the CA target, impact plasmas generated there are separated much faster than impact plasmas formed on the IIT. Thus, impacts onto the CA target are characterised by small rise times. The efficiency of collecting plasma ions at the ion grid is higher for CAT impacts than for IIT impacts (CAT: $q_{QC}/q_{QI} \sim 3 \ldots 6$, IID: $q_{QT}/q_{QI} \sim 6 \ldots 12$, see also Fig. 3.1 and 3.2). Furthermore, impacts on the CA target lead to a TOF line spectrum unless the particle hits the CAG. Since the transmission of the acceleration grid is 68%, one third of the impacts within the CA field-of-view will occur on the CAG. Such impacts cause a short negative QT feature shortly after the instant of impact and do not lead to a TOF spectrum. In what follows, impacts onto the CA target are called CAT impacts, while impacts onto the CA grid are called CAG impacts.

As said before, the site of impact needs to be known to employ the correct set of calibration relations for determining the impact speed and dust mass. The set of criteria for identifying the impact target are:

- A clear TOF line spectrum indicates a dust impact on the CAT

- In most cases the larger fraction of the total (negative) impact charge is released on the target stroke by the dust grain, i.e. $q_{QT} > q_{QC}$ implies an IIT impact

- CAT impacts typically have charge yield ratios of $q_{QC}/q_{QI} \sim 3 \ldots 6$

- IIT impacts typically have charge yield ratios of $q_{QT}/q_{QI} \sim 6 \ldots 12$
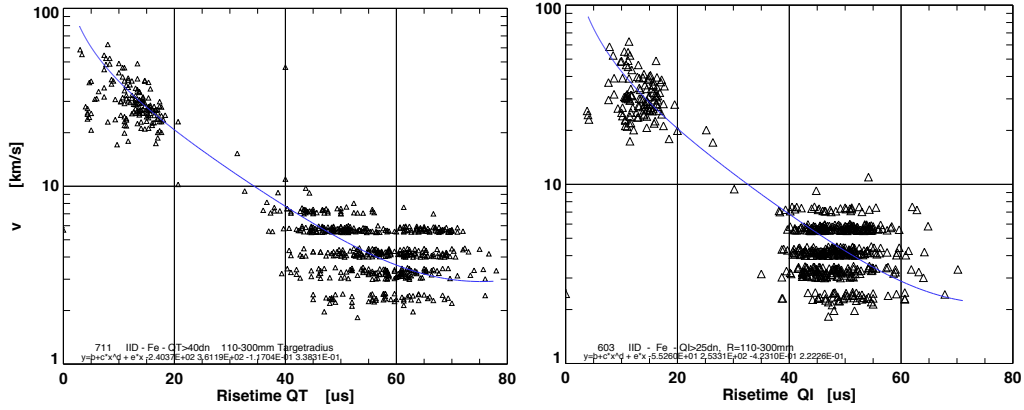
Figure 3.4.: Dependence of the signal rise time on the dust impact speed for iron par-
ticle impacts on the IIT. The blue lines show the fits to the data using the
speed calibration functions Eqs. (3.2) and (3.1). **Left:** Rise time of the
electron charge monitored by the QT electrode. **Right:** Rise time of the
ion charge monitored by the QI electrode. The banded structure of the
calibration data is a consequence of the dust accelerator's Particle Selec-
tion Unit (PSU), which allows the experimenter to investigate dust impacts
within a narrow impact speed range.

- CAT impacts typically have very short rise times ($t_{QC} < 10\,\mu s$, $t_{QI} < 10\,\mu s$) even
at low impact speeds

Note that this set of criteria is not always conclusive. In particular, energetic impacts
(fast impacts of large dust grains) we cause strong crosstalk between the amplifiers.
Hypervelocity impacts of nano grains may only produce a faint QI signal and a very
faint mass spectrum showing a single mass line. On the other hand, impact ejecta may
strike the CAT and produce a mass spectrum although the primary impact happened
on the IIT.

3.2. Determination of the impact speed

The determination of the dust impact speed from the properties of the produced im-
pact plasma is rather inaccurate. The dust impact generates a primary charge signal
(electrons and ions of the primary impact plasma) and a secondary charge signal due
to secondary impacts of fragments and ejecta produced by the primary impact. The
ejecta have speeds of a few $km\,s^{-1}$ and a broad emission angle. The impact plasma
of the primary and secondary impacts are collected by the electrodes attached to the
impact target. The faster the dust impact, the more primary charge is generated, cor-
responding to a more rapid increase of the total impact charge collected at the target.
This fact constitutes the basic principle of speed calibration of impact ionisation de-
tectors. The evolution time of the impact plasma is characterized by the rise time t_r,

Figure 3.5.: Distribution of the speed calibration error factors, defined as the ratio between the true impact velocity and the velocity derived via Eqs. (3.2) or (3.1). **Left:** Error factor distribution for speeds derived from the QT signals. **Right:** Error factor distribution for speeds derived from the QI signals.

which is defined as the time between 10% and 90% of the signal amplitude.

Srama (2010) performed extensive calibration campaigns with the CDA flight spare unit using iron grains in the Heidelberg accelerator facility. Fig. 3.4 shows the dependence of the rise time (determined for both, the electron charge measured by the QT electrode and the ion charge measured by the QI electrode) on the impact speed. The apparent lack of impact data with speeds between 10 and 16 km s^{-1} is because of the fact that electrostatic dust accelerators are very inefficient to provide large fast dust particles. However, the two data point clouds are also at least partially due to the physics of hypervelocity impacts, because slow impacts produce small amount of primary impact plasma (corresponding to long rise times), while fast impacts produce a large primary impact charge (short rise times).

The best fit to the speed calibration data shown in Fig. 3.4 is

$$v_{QI} = -55 + 253 t_{QI}^{-0.423} + 0.222 t_{QI} \tag{3.1}$$

$$v_{QT} = -240 + 361 t_{QT}^{-0.117} + 0.338 t_{QT}, \tag{3.2}$$

with t_r in μs and v_d in km s^{-1} (Srama, 2010). The logarithmic ratios e_v of the true impact speeds v_{true} and the speed estimates derived from the plasma rise time are normal distributed (see Fig. 3.5), i.e. $N(\ln e_v) = 1/\sigma_v \sqrt{2\pi} \exp(-\frac{1}{2}(\ln e_v/\sigma_v)^2)$. This implies that the accuracy of the rise time method is described best by an error factor $\Delta_v = e^{\sigma_v}$. This means that 68% of the speed estimates lie within the interval $\{v_{true}/\Delta_v, v_{true} \cdot \Delta_v\}$. The error factor of the rise time method is $\Delta_v \approx 1.6$. In principle, the accuracy of the speed estimates derived from the QT and QI signals are comparable, and one
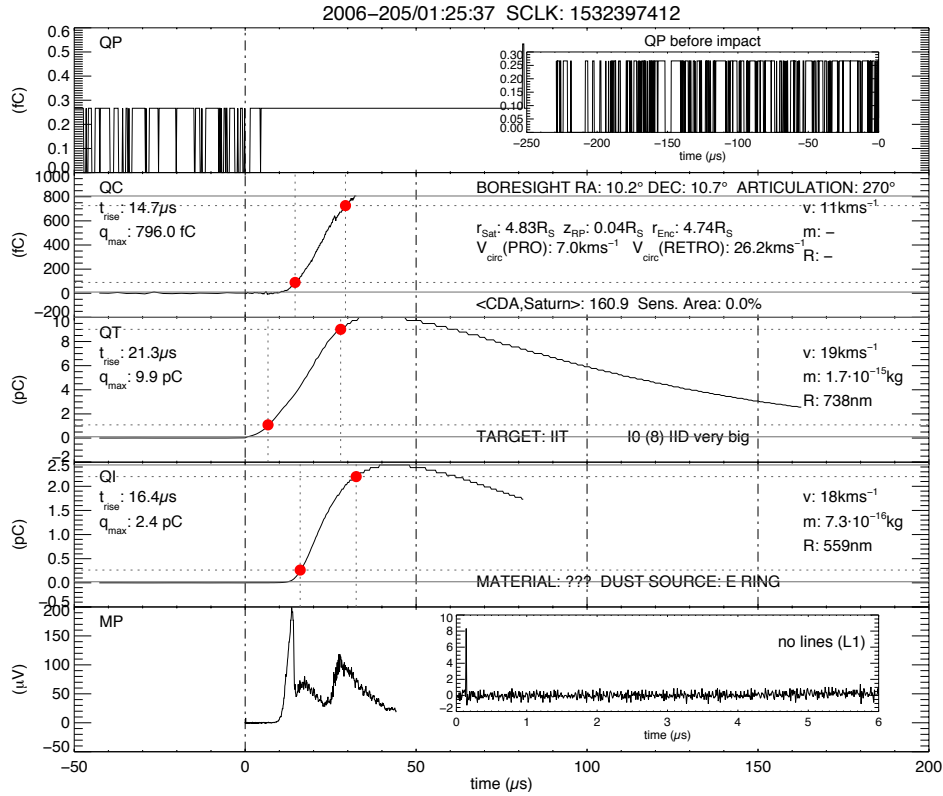
Figure 3.6.: Typical example for an impact onto the IIT. The red dots mark the times at 10% and 90% of the maximum amplitude, respectively.

may therefore arrive at the conclusion that the speed calibration should be based on a weighted average of v_{QI} and v_{QI}. However, this approach leads to less accurate speed estimates because the resulting error factor is $(\Delta_v)^2 \approx 2.6$. We consider it to be good practice to base the speed calibration on the QI signal.

Sometimes, more accurate impact speed estimates are available, such as speeds derived from the QP signal or from the appearance of a mass spectrum. For data obtained in dust-rich environments such as Saturn's E ring, the impact speed of particles moving in circular Keplerian orbit is often a better estimator for the true impact speed than speeds derived from the signal rise times.

3.2.1. Example case

Fig. 3.6 shows a typical example of an impact of a E ring particle onto the IIT obtained in 2006. The particle has been detected at a radial distance to Saturn of $4.74R_S$ (Saturn's radius $R_S = 60330$km). At this distance, the impact speed of a ring particle moving in a prograde, circular Keplerian orbit is $v_d = 7.0$km s^{-1}, while the speed of a grain moving in a retrograde, circular is $v_d = 26.2$km s^{-1}. Impact speeds of eccentric
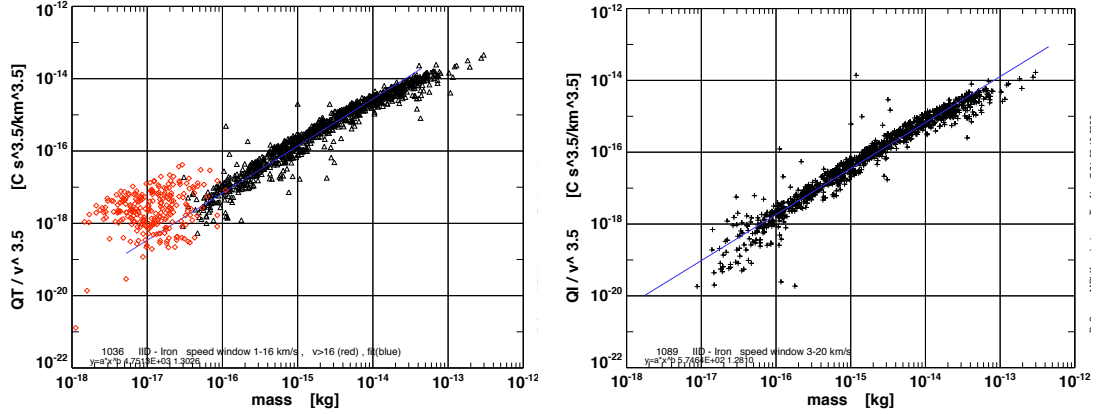
Figure 3.7.: Dependence of the impact speed-weighted charge yield $q/v_d^{3.5}$ on the impactor's mass for iron particle impacts on the IIT. The red symbols mark impacts faster than 16km s^{-1}. The blue lines show the fits to the data using the mass calibration functions Eqs. (3.3) and (3.4). **Left:** $q_{QT}/v_d^{3.5}$ versus m_d **Right:** $q_{QI}/v_d^{3.5}$ versus m_d

grains may be significantly faster or slower than the given values.

The shown set of signals fulfills the requirements for an impact onto the IID (see 3.1.2). The multiplier signal doesn't show a TOF spectrum characteristic for an impact onto the CAT. Furthermore, $q_{QT} \gg q_{QC}$ implies that most of the impact charge has been produced on the IIT, while the small amount of impact plasma released on the CAT is due to impact ejecta. The ratio between the electron and ion charge yield of ≈ 4.4 is rather low but not inconsistent with an IIT impact.

The rise time is defined as the time interval between 10% and 90% of a channel's amplitude. For the impact considered here the rise times are $t_{QI} = 16.4\,\mu s$, $t_{QC} = 14.7\,\mu s$, and $t_{QT} = 21.3\,\mu s$. Using the calibration relations (3.1) and (3.2), the impact speed is found to be $\log(v_{QI}) = \log(18 \text{km s}^{-1}) \pm \log(1.6)$ and $\log(v_{QT}) = \log(19 \text{km s}^{-1}) \pm \log(1.6)$, respectively. This means that the 1-σ interval for the impact speed is about $11 \text{km s}^{-1} \leq v_d \leq 29 \text{km s}^{-1}$.

Obviously, the derived impact speed is not compatible with a ring particle moving in a circular orbit. However, because of the instrument's orientation at the time of impact, the event cannot be due to a retrograde ring particle. Thus, the impact is most likely due to a particle moving in an eccentric prograde orbit, detected close to its pericenter.

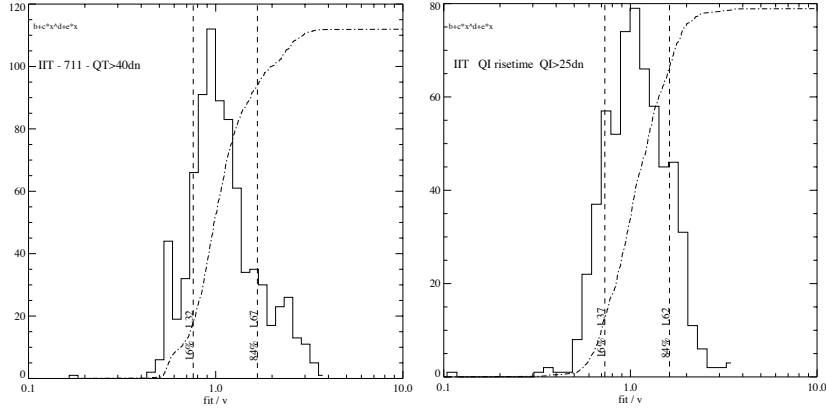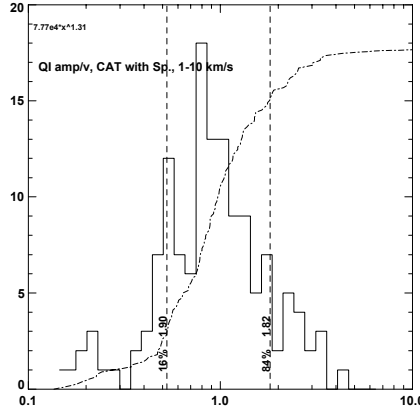**Figure 3.8.:** Distribution of the mass calibration error factors, defined as the ratio between the true dust mass and the mass derived via Eq. (3.4) from the QI charge yield (using the correct impact speed).

3.3. Determination of the impactor mass

The relationship between the impact charge q, the dust speed v_d and the dust mass m_d is well studied and the basis of the CDA mass determination. The larger the dust grain the more impact charge is generated. Furthermore, the faster the impact speed, the greater is the impact charge. Usually, the charge yield scales linearly with the dust mass; whereas the dependence on the impact speed is much steeper than the speed dependence of the grain's kinetic energy. The typical exponent b of the speed dependence of the impact charge is about 3.5. For this reason, impact calibration data are traditionally plotted as m_d versus $q/v_d^{3.5}$ (Fig. 3.7). The best fit to the calibration data is

$$q_{QT} = 4751 m_d^{1.3} v_d^{3.5} \quad \text{or} \quad m_d = \frac{q_{QT}^{0.769}}{672 v_d^{2.69}} \tag{3.3}$$

$$q_{QI} = 575 m_d^{1.28} v_d^{3.5} \quad \text{or} \quad m_d = \frac{q_{QI}^{0.781}}{143 v_d^{2.73}} \tag{3.4}$$

for impacts onto the IIT, where the speeds and masses are given in $\mathrm{km\,s^{-1}}$ and kg, respectively. The calibration data clearly supports the $v_d^{3.5}$ dependence of the impact charge. However, it has to be noted that only impacts slower than $20\mathrm{km\,s^{-1}}$ have been considered here. Higher impact speeds do not comply with the fits given by (3.3) and (3.4). Stübig (2002) found speed exponents of only 2 for higher impact speeds.

The error statistics of the mass calibration is very similar to the statistics of the speed calibration (see Sec. 3.2). Here the distribution of the logarithmic ratios between the true impactor mass m_{true} and the mass estimates derived from the impact charge matches a normal distribution as well. Srama (2010) determined the error factor of the

CDA mass calibration as $\Delta_m \approx 1.8$. Note that Δ_m is the mass error factor for impacts for which the impact speed is known. In fact, the mass error factor is $\Delta_{m,v} = \Delta_m \Delta_v^{3.5} \approx 9.3$, if the impact speed has been derived from the plasma rise time.

3.3.1. Example case

As example we return to the dust impact we already considered in Sec. 3.2. The wave forms of the plasma signals are shown in Fig. 3.6. The plasma charge yields are $q_{QT} = 9.9$pC and $q_{QI} = 2.4$pC. We already estimated the impact speed to be about 18km s^{-1}. Using Eqs. (3.3) and (3.4) and assume that $v_d = 18$km s^{-1} we find that $m_{QT} = 1.7 \cdot 10^{-15}$kg and $m_{QI} = 7.3 \cdot 10^{-16}$kg. Because we used a rise time speed estimate the 1-σ intervals for the dust mass are $1.7 \cdot 10^{-16}$kg $\leq m_{QT} \leq 1.7 \cdot 10^{-14}$kg and $7.3 \cdot 10^{-17}$kg $\leq m_{QT} \leq 7.3 \cdot 10^{-15}$kg, respectively. Obviously, the two mass estimates are consistent. Note that the dust size can be estimated much more accurately. Assuming spherical water ice particles one finds that $s_{QI} \approx 560$ nm with an error factor of $\Delta_{m,r}^{1/3} \approx 2.1$.

4. Determination of impact rate and dust flux

4.1. Correction for incomplete data sets

Usually the data rates are sufficient to transmit the complete raw data sets to Earth. As described in Section 1.4, the CDA flight software associates each event registered by the instrument with an "event type" and transmits every 32 seconds snapshots of the counting states to the Earth . To determine the number of dust impacts registered by CDA during two successive counter snapshots, the counter states need to be correlated with the properties of the impactors derived from the incompletely transmitted raw data. To this aim, for each transmitted event the mass m_d and impact speed v_d is derived as described in Sections 3.2 and 3.3.

Now, let $N_c(t)$ the number of events of type c detected during two consecutive counter snapshots at t and $t + \Delta t$, $N_c^t(t)$ the number of transmitted c-type events, and $N_c^t(t, m_d)$ the number of transmitted c-type events caused by impactors of mass m_d. Then, the number of impacts of grains of this mass is approximately

$$N(t, m_d) \approx \sum_{c=1}^{26} w_c(t, m_d) N_c^t(t, m_d), \tag{4.1}$$

where

$$w_c(t) = \begin{cases} \frac{N_c(t)}{N_c^t(t)} & : N_c^t(t) > 0 \\ 0 & : N_c^t(t) = 0 \end{cases} \tag{4.2}$$

is the transmission correction factor.

4.1.1. Example case

As an example let us consider data obtained during the third Rhea flyby in 2011. Tab. 4.1 shows 4 consecutive counter snapshots together with the number of transmitted events caused by dust impacts onto the IIT which produced an ion impact charge $q_{QI} \geq 300\text{fC}$. The flight software associated those events with 7 event types (I0, I1, I2, I3, I4, I5, and W1; the event type definitions are given in Tab. 1.4). It is important to understand that this fact does not imply that this group of event types only contains events by the impactor type considered in this example. It should also be understood

Table 4.1.: Snapshots N_c of the CDA event type counters listed together with the number N_c^t of transmitted events caused by IIT impacts with $q_{QI} \geq 300$fC and the corresponding transmission correction factor w_c. Shown are 4 consecutive snapshots recorded between 2011-011/04:45:11 and 2011-011/04:49:27; the time increment is 64 s. Event counters which did not increased during the time interval shown here are not included. The bottom row gives the estimated number $N(t) = \sum N_c(t) w_c(t)$ of IIT events fulfilling the condition $q_{QI} \geq 300$fC.

c		04:45:11			04:46:15			04:47:19			04:48:23		
		N_c	N_c^t	w_c	N_c	N_c^t	w_c	N_c	N_c^t	w_c	N_c	N_c^t	w_c
8	I0	0	0	0.00	0	1	0.00	1	0	0.00	1	0	0.00
9	I1	0	0	0.00	0	0	0.00	1	0	0.00	1	0	0.00
10	I2	2	2	1.00	3	0	0.00	2	1	2.00	0	0	0.00
11	I4	11	1	11.00	13	2	6.50	11	2	5.50	9	4	2.25
12	I5	0	0	0.00	3	1	3.00	3	0	0.00	1	0	0.00
17	I3	2	2	1.00	2	2	1.00	3	3	1.00	2	2	1.00
21	W1	5	5	1.00	3	3	1.00	5	5	1.00	3	3	1.00
N			20			21			21			14	

that the event type assigned by the flight software can be misleading. As an example, the instrument registered during the time interval considered here not a single wall impact despite the 19 "wall impact events" reported by the counter W1.

The last row of Tab. 4.1 gives the estimated number $N(t)$ of IIT events with $q_{QI} \geq 300$fC calculated using (4.1).

4.2. Dead time correction of the impact rate

When a DA measurement is triggered by either a noise event or by a genuine impact, the instrument cannot respond to another trigger until it finalises its data processing. The time needed for measurement is controlled by real time interrupts (RTIs) broadcasted eight times per second, at constant intervals, on the spacecraft bus. Once it starts a measurement cycle, the DA becomes sensitive again only after receiving eight RTIs (see Fig. 4.1). Thus, the instrument dead time ranges between

$$\tau_{min} = 7\Delta \leq \tau \leq 8\Delta = \tau_{max},$$

where $\Delta = 1/8$ s, and τ_{min} and τ_{max} are the minimum and the maximum dead time. As a consequence of the finite instrument response time to an event trigger, the registered number of events $N(T)$ throughout the time interval T is mostly smaller than the true number of impacts.
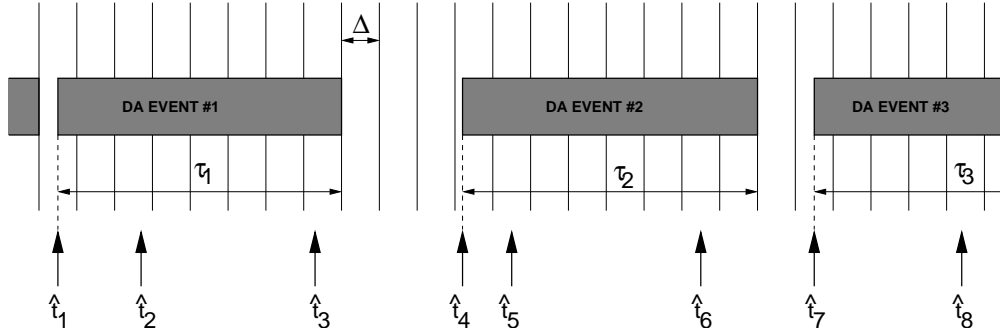
Figure 4.1.: Visualisation of the DA response to dust impacts. Vertical lines mark the RTI synchronisation pulses with the period Δ, while arrows indicate a possible realisation of a dust impact time sequence. Once the DA is triggered by an impact the instrument is insensitive to dust impacts for at least 7 RTI cycles. Here, only the impacts at $\hat{t}_1$, $\hat{t}_4$, and $\hat{t}_7$ were registered, i.e. the number of detected events is $N = 3$ although the instrument experiences 8 event triggers during the shown time interval T caused by a Poisson process with the average event rate $r = 8/T$.

The effect of the instrument dead time on the number of registered events can be estimated from the rate-dependent statistics of the dead time τ. Kempf (2008) found that the expectation value and the variance of the deadtime are

$$\bar{\tau}(r) = \tau_{max} - r^{-1} + \Delta \left(e^{r\Delta} - 1 \right)^{-1} \tag{4.3}$$

and

$$\sigma_\tau^2(r) = r^{-2} - \Delta^2 e^{r\Delta} \left(e^{r\Delta} - 1 \right)^{-2}. \tag{4.4}$$

Fig. 4.2 shows $\bar{\tau}$ for impact rates between 1 and 5000 impacts per minute. At very small rates r, $\bar{\tau} \sim \tau_m - \Delta/2 = 7.5\Delta$ and $\sigma_\tau^2 \sim \Delta/12$. At large rates, $\bar{\tau}(r) \sim \tau_{max} - r^{-1}$ and $\sigma_\tau^2 \sim r^{-2} - \Delta^2 e^{-\Delta r}$, implying that on average the instrument is re-triggered after the mean time interval between two events. Note also that $\bar{\tau}$ asymptotically approaches its maximum value τ_{max} as the impact rate increases. The most probable impact rate corresponding with N impacts detected by the DA throughout T is then

$$\mu_r(N) = \Delta^{-1} \ln \left(\frac{T - N\tau_{min}}{T - N\tau_{max}} \right) \quad \text{with } N < T/\tau_{max}. \tag{4.5}$$

The instrument will be saturated, if the impact rate exceeds

$$\mu_{rmax}(T) \approx \Delta^{-1} \ln \left(\frac{T\Delta + \tau_{min}\tau_{max}}{\tau_{max}^2} \right). \tag{4.6}$$

However, because $\mu_{rmax}(T)$ increases with the "time bin" T, the time grid can always be chosen such that $\mu_r(N) < \mu_{rmax}(T)$.
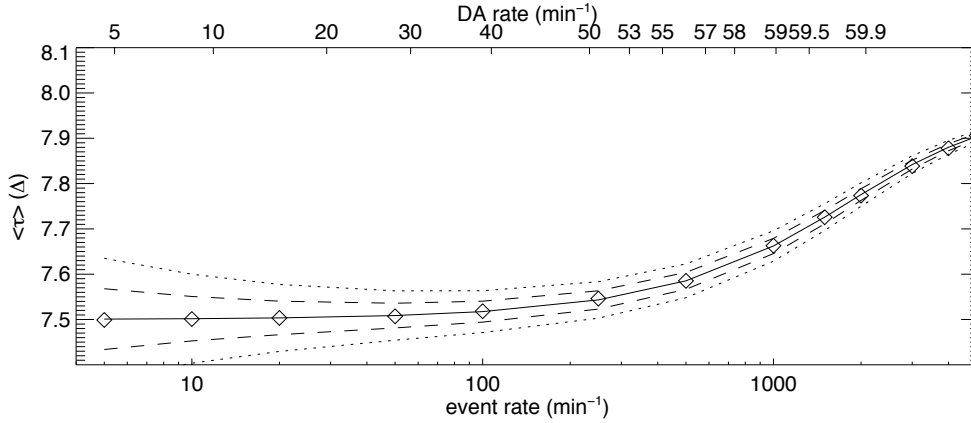
Figure 4.2.: Mean dead time (Eq. (4.3)) plotted against the true event rate as well as against the DA rate. The mean deviation $\sigma_\tau(r, T)$ from $\bar{\tau}$ is shown as well (dotted lines: $T = 1$ min measurement, broken lines; $T = 4$ min). The diamonds are values derived from MC simulations. From (Kempf et al., 2008).

4.2.1. Example

As an example we consider DA data taken during a traversal of Cassini through Saturn's E ring on 2005-177 13:29 UTC (Fig. 4.3). The spacecraft pierced the ring plane at a radial distance to Saturn of $3.94 R_S$ (Saturn radius $R_S = 60330$km). Because the ring plane crossing was very steep, the rate profile should resemble the Gaussian vertical profile of the E ring. The uppermost panel of Fig. 6 shows the total number of DA events registered within 64s as function of the time. N was almost continuously only slightly smaller than the maximum event number $N_{max} = 64$. There is no apparent indication for a Gaussian rate profile. However, after performing the dead time correction as described in this section a pronounced profile shows up (see Fig. 4.3 b-e). On short observation time scales the instrument was frequently saturated (saturation periods are marked by shaded areas). On longer time scales the saturation periods vanish and the rate curve becomes smoother. Note that for $T = 264$s (Fig. 4.3 d) only one saturation period remained which coincides with the time of the ring plane crossing.

The comparison between rates derived for different time scales provides a powerful criterion for discriminating between rate features caused by spatial and temporal fluctuations of the dust environment and genuine features. Note that it was implicitly assumed that the mean impact rate onto the DA is constant throughout the observation period T. In this case the rates derived on a shorter time scale must lie within the variation range of the rate derived on the longer time scale, i.e.:

$$\mu_r(T,t) - \sigma_r(T,t) \le \mu_r(T',t') \le \mu_r(T,t) + \sigma_r(T,t) \quad \text{with} \, t \le t' \le t + T.$$

A violation of this condition means that variations of $\mu_r(T',t')$ throughout the interval T cannot be attributed to Poissonian fluctuations of the rate around the expectation
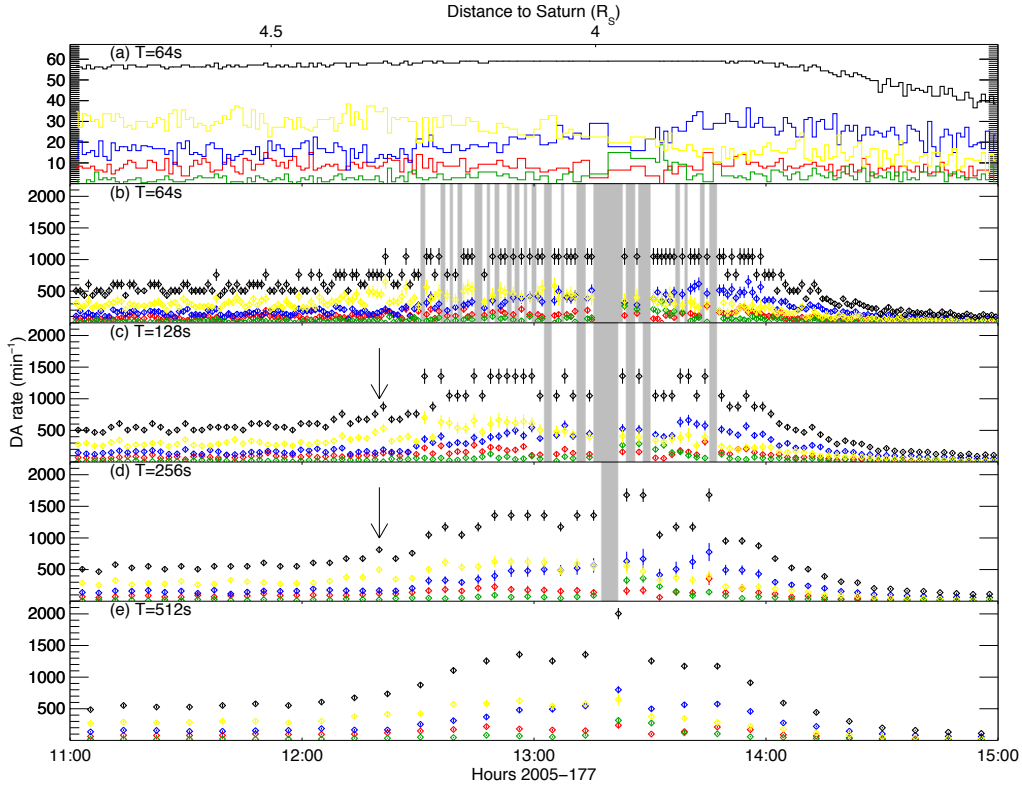
Figure 4.3.: DA impact rate measured around the ring plane crossing on 2005-177 13:29 UTC plotted for different values of T and corrected for dead time effects. For comparison, the uppermost panel displays the uncorrected DA rate. In each panel the total impact rate (black), the rate of big target impacts (blue), the rate of small target impacts (red), the wall impact rate (green), and the rate of noise events (yellow) are shown. Grey areas mark periods when the total number of events N detected within T equals $T \cdot 1\,\mathrm{sec}$.

value $\mu_r(T)$. As an example the feature marked in Fig. 4.3 is caused by an genuine variation of the dust density on a time scale of $\sim 256\,\mathrm{s}$ corresponding with a spatial scale of $4\,200\,\mathrm{km}$.

4.3. Sensitive Area

The effective sensitive area of CDA depends on the orientation of the impact target to the direction of the dust flux. Srama (2010) performed Monte Carlo simulations to determine the dependence of the sensitive area of the IIT, CAT, and the inner walls on the dust incidence angle θ. The sensitivity decreases for increasing incidence angles. The CAT does not detect any impacts with incidence angles larger than $\pm 28°$ and the maximum incidence angle for ITT impacts is $\pm 45°$. These limits are due to the
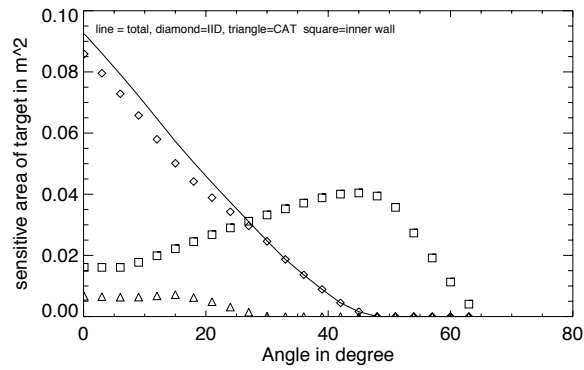
Figure 4.4.: Dependence of the detector's sensitive area on the dust incidence angle θ. Shown is the sensitivity of the IIT (◇), CAT (△), and the multiplier housing (□).

shielding by the side walls of the detector cone. The simulations took the obscuration of the multiplier housing and struts into account. This explains why the CAT sensitivity is not maximum for normal incidence (θ = 0°). The tabulated simulation data shown in Fig. 4.4 allow the user to compute for a known (or assumed) dust impact angle to compute the instrument's sensitive area.

Bibliography

Auer, S., 1975. Two high resolution velocity vector analyzers for cosmic dust particles. Rev. Sci. Instrum. 46, 127–135.

Auer, S., 2001. Instrumentation, in: Grün, E., Gustafson, B., Dermott, S., Fechtig., H. (Eds.), Interplanetary Dust. Springer, pp. 387–438.

Auer, S., Grün, E., Srama, R., Kempf, S., Auer, R., 2002. The charge and velocity detector of the Cosmic Dust Analyser on Cassini. Planet. Space Sci. 50, 773–779.

Eichhorn, G., 1978. Primary velocity dependence of impact ejecta parameters. Planet. Space Sci. 26, 469–471.

Göller, J.R., Grün, E., 1989. Calibration of the Galileo/Ulysses dust detectors with different projectile materials and at varying impact angles. Planet. Space Sci. 37, 1197–1206.

Grün, E., Fechtig, H., Hanner, M.S., Kissel, J., Lindblad, B.A., Linkert, D., Maas, D., Morfill, G.E., Zook, H.A., 1992a. The Galileo Dust Detector. Space Science Reviews 60, 317–340.

Grün, E., Fechtig, H., Kissel, J., Linkert, D., Maas, D., McDonnell, J.A.M., Morfill, G.E., Schwehm, G., Zook, H.A., Giese, R.H., 1992b. The Ulyssses dust experiment. Astron. Astrophys. Sup. 92, 411–423.

Grün, E., Kempf, S., Srama, R., Moragas-Klostermeyer, Altobelli, N., 2002. Analysis of impact ionization from 300 km/s fast projectiles, in: Geophysical Research Abstracts, EGS.

Hillier, J.K., McBride, N., Green, S.F., Kempf, S., Srama, R., 2006. Modelling CDA mass spectra. Planet. Space Sci. 54, 1007–1013.

Kempf, S., 2008. Interpretation of high rate dust measurements with the Cassini dust detector CDA. Planet. Space Sci. 56, 378–385.

Kempf, S., Beckmann, U., Moragas-Klostermeyer, G., Postberg, F., Srama, R., Economou, T., Schmidt, J., Spahn, F., Grün, E., 2008. The E ring in the vicinity of Enceladus I: Spatial distribution and properties of the ring particles. Icarus 193, 420–437.

Bibliography

Kempf, S., Srama, R., Altobelli, N., Auer, S., Tschernjawski, V., Bradley, J., Burton, M., Helfert, S., Johnson, T., Krüger, H., Moragas-Klostermeyer, G., Grün, E., 2004. Cassini between Earth and asteroid belt: First in-situ charge measurements of interplanetary grains. Icarus 171, 317–335.

Kempf, S., Srama, R., Horányi, M., Burton, M., Helfert, S., Moragas-Klostermeyer, G., Roy, M., Grün, E., 2005. High-velocity streams of dust originating from Saturn. Nature 433, 289–291.

Postberg, F., Kempf, S., Hillier, J.K., Srama, R., Green, S.F., McBride, N., Grün, E., 2008. The E-ring in the vicinity of Enceladus II: Signatures of Enceladus in the elemental composition of E-ring particles. Icarus 193, 438–454.

Postberg, F., Kempf, S., Srama, R., Green, S.F., Hillier, J.K., McBride, N., Grün, E., 2006. Composition of jovian dust stream particles. Icarus 183, 122–134.

Ratcliff, P., Gogu, F., Grün, E., Srama, R., 1995. Plasma production by secondary impacts: implications for velocity measurements by in-situ dust detectors. Adv. Space Res. 17, 111–115.

Simpson, J.A., Tuzzolino, A.J., 1985. Polarized polymer films as electronic pulse detectors of cosmic dust particles. Nucl. Instrum. Methods A 236, 187–202.

Srama, R., 2000. CDA calibration report. Technical Report. MPI-K.

Srama, R., 2010. Cassini–Huygens and Beyond – Tools for Dust Astronomy. Ph.D. thesis. Universität Stuttgart.

Srama, R., Ahrens, T.J., Altobelli, N., Auer, S., Bradley, J.G., Burton, M., Dikarev, V.V., Economou, T., Fechtig, H., Görlich, M., Grande, M., Graps, A., Grün, E., Havnes, O., Helfert, S., Horanyi, M., Igenbergs, E., Jessberger, E.K., Johnson, T.V., Kempf, S., Krivov, A.V., Krüger, H., Mocker-Ahlreep, A., Moragas-Klostermeyer, G., Lamy, P., Landgraf, M., Linkert, D., Linkert, G., Lura, F., McDonnell, J.A.M., Möhlmann, D., Morfill, G.E., Müller, M., Roy, M., Schäfer, G., Schlotzhauer, G., Schwehm, G.H., Spahn, F., Stübig, M., Svestka, J., Tschernjawski, V., Tuzzolino, A.J., Wäsch, R., Zook, H.A., 2004. The Cassini Cosmic Dust Analyzer. Space Science Reviews 114, 465–518.

Stübig, M., 2002. New insights in impact ionization and in time-of-flight mass spectroscopy with micrometeoroid detectors by improved impact simulations in the laboratory. Ph.D. thesis. Heidelberg University.

A. Acronyms and Abbreviations

ASCII	American Standard Code for Information Interchange
CA	(CDA) Chemical Analyzer
CAG	(CDA)Chemical Analyzer Grid
CAPS	Cassini Plasma Spectrometer
CAT	(CDA)Chemical Analyzer Target
CDA	Cosmic Dust Analyzer
CDU	Charge Detection Unit
CER	Corotation eccentricity resonance
CIR	Co-rotating interaction region
CME	Coronal Mass Ejection
DA	Dust Analyzer
DN	Digital number (units)
DLA	??
ESB	Earth Swing By (manoeuvre)
FSW	Flight Software
FWHM	Full Width Half Maximum
HGA	High Gain Antenna
HRD	High Rate Detector
IDD	Initial Delivery Date
IDP	Interplanetary Dust Particle
IID	Impact Ionization Target
IIT	Impact Ionisation Detector Target
IMF	Interplanetary Magnetic Field
INMS	(Cassini) Ion and Neutral Mass Spectrometer
ISD	Interstellar Dust
JD	Julian Day
JPL	Jet Propulsion Laboratory
LIFO	last in first out (organised memory)
LOS	Line of Sight
LP (RPWS)	Langmuir Probe
LSB	Least Significant Byte
MAG	Cassini Magnetometer
MIMI	Magnetospheric Imaging Instrument
MP	(CDA) Multiplier
MPI-K	Max Planck Institut für Kernphysik
MSB	Most Significant Byte

A. Acronyms and Abbreviations

NASA	National Aeronautics and Space Administration
NEP	North Ecliptic Pole
ODL	Object Description Language
PDS	Planetary Data System
QP	(CDA) Charge Sensor
RADAR	Cassini Radar
RPWS	Radio and Plasma Wave Science Investigation
RSS	Radio Science Subsystem
S/C	Spacecraft
SBN	Small Bodies Node
SCLK	Spacecraft Clock
SEP	South Ecliptic Pole
SFDU	Standard Formatted Data Unit
SIS	Software Interface Specification
SNR	Signal-to-noise ratio
SOI	Saturn Orbit Insertion
TBD	To Be Determined
TOF	Time of Flight
UT	Universal Time
UTC	Universal Time Coordinated

B. Published literature that would be applicable to understanding the data or its processing

Ahrens, J., Gupta, S., Jyoti, G., Beauchamp, J., 2003. Mass spectrometer calibration of cosmic dust analyzer. *J. Geophys. Res.* **108**.

Altobelli, N., Dikarev, V., Kempf, S., Srama, R., Helfert, S., Moragas-Klostermeyer, G., Roy, M., Grün, E., 2007. Cassini/Cosmic Dust Analyzer in situ dust measurements between Jupiter and Saturn. *J. Geophys. Res.* **112**, 7105.

Altobelli, N., Kempf, S., Landgraf, M., Srama, R., Dikarev, V., Krüger, H., Moragas-Klostermeyer, G., Grün, E., 2003. Cassini between Venus and Earth: Detection of interstellar grains. *J. Geophys. Res.* **108**,8032.

Auer, S., 1975. Two high resolution velocity vector analyzers for cosmic dust particles. *Rev. Sci. Instrum.* **46**, 127–135.

Instrumentation, in: Grün, E., Gustafson, B., Dermott, S., Fechtig., H. (Eds.), Interplanetary Dust. Springer, pp.387–438.

Auer, S., Grün, E., Srama, R., Kempf, S., Auer, R., 2002. The charge and velocity detector of the Cosmic Dust Analyser on Cassini. *Planet. Space Sci.* **50**, 773–779.

Eichhorn, G., 1978. Primary velocity dependence of impact ejecta parameters. *Planet. Space Sci.* **26**, 469–471.

Goldsworthy, B.J., Burchell, M.J., Cole, M.J., Armes, S.P., Khan, M.A., Lascelles, S.F., Green, S.F., McDonnell, J.A.M., Srama, R., Bigger, S.W., 2003. Time of flight mass spectra of ions in plasmas produced by hypervelocity impacts of organic and mineralogical microparticles on a cosmic dust analyser. *Astron. Astrophys.* **409**, 1151–1167.

B. Published literature that would be applicable to understanding the data or its processing

Henry, C.A., 2002. An Introduction to the Design of the Cassini Spacecraft. *Space Science Reviews* **104**, 129–153.

Hillier, J.K., Green, S.F., McBride, N., Altobelli, N., Postberg, F., Kempf, S., Schwanethal, J., Srama, R., McDonnell, J.A.M., Grün, E., 2007a. Interplanetary dust detected by the Cassini CDA Chemical Analyser. *Icarus* **190**, 643–654.

Hillier, J.K., Green, S.F., McBride, N., Schwanethal, J.P., Postberg, F., Srama, R., Kempf, S., Moragas-Klostermeyer, G., McDonnell, J.A.M., Grün, E., 2007b. The composition of Saturn's E ring. *Mon. Not. Roy. Astron. Soc.* **377**, 1588–1596.

Hillier, J.K., McBride, N., Green, S.F., Kempf, S., Srama, R., 2006. Modelling CDA mass spectra. *Planet. Space Sci.* **54**, 1007–1013.

Hillier, J.K., Sestak, S., Green, S.F., Postberg, F., Srama, R., Trieloff, M., 2009. The production of platinum-coated silicate nanoparticle aggregates for use in hypervelocity impact experiments. *Planet. Space Sci.* **57**, 2081–2086.

Kempf, S., 2008. Interpretation of high rate dust measurements with the Cassini dust detector CDA. *Planet. Space Sci.* **56**, 378–385.

Kempf, S., Beckmann, U., Moragas-Klostermeyer, G., Postberg, F., Srama, R., Economou, T., Schmidt, J., Spahn, F., Grün, E., 2008a. The E ring in the vicinity of Enceladus I: Spatial distribution and properties of the ring particles. *Icarus* **193**, 420–437.

Kempf, S., Beckmann, U., Schmidt, J., 2010. How the Enceladus dust plume feeds Saturn's E ring. *Icarus* **206**, 446–457.

Kempf, S., Beckmann, U., Srama, R., Horanyi, M., Auer, S., Grün, E., 2006. The electrostatic potential of E ring particles. *Planet. Space Sci.* **54**, 999–1006.

Kempf, S., Srama, R., Altobelli, N., Auer, S., Tschernjawski, V., Bradley, J., Burton, M., Helfert, S., Johnson, T., Krüger, H., Moragas-Klostermeyer, G., Grün, E., 2004. Cassini between Earth and asteroid belt: First in-situ charge measurements of interplanetary grains. *Icarus* **171**, 317–335.

Kempf, S., Srama, R., Horányi, M., Burton, M., Helfert, S., Moragas-Klostermeyer, G., Roy, M., Grün, E., 2005a. High-velocity streams of dust originating from Saturn. *Nature* **433**, 289–291.

Kempf, S., Srama, R., Postberg, F., Burton, M., Green, S.F., Helfert, S., Hillier, J.K., McBride, N., McDonnell, J.A.M., Moragas-Klostermeyer, G., Roy, M., Grün, E., 2005b. Composition of saturnian stream particles. *Science* **307**, 1274–1276.

B. Published literature that would be applicable to understanding the data or its processing

Lavila, P., 2002. Analyzing Time-of-Flight Spectra of CDA. Research report. Max Planck Institut für Kernphysik.

Postberg, F., Kempf, S., Hillier, J.K., Srama, R., Green, S.F., McBride, N., Grün, E., 2008. The E-ring in the vicinity of Enceladus II: Signatures of Enceladus in the elemental composition of E-ring particles. *Icarus* **193**, 438–454.

Postberg, F., Kempf, S., Rost, D., Stephan, T., Srama, R., Trieloff, M., Mocker, A., Goerlich, M., 2009a. Discriminating contamination from particle components in spectra of Cassini's dust detector CDA. *Planet. Space Sci.* **57**, 1359–1374.

Postberg, F., Kempf, S., Schmidt, J., Brilliantov, N., Beinsen, A., Abel, B., Buck, U., Srama, R., 2009b. Sodium salts in E-ring ice grains from an ocean below the surface of Enceladus. *Nature* **459**, 1098–1101.

Postberg, F., Kempf, S., Srama, R., Green, S.F., Hillier, J.K., McBride, N., Grün, E., 2006. Composition of jovian dust stream particles. *Icarus* **183**, 122–134.

Ratcliff, P., Gogu, F., Grün, E., Srama, R., 1995. Plasma production by secondary impacts: implications for velocity measurements by in-situ dust detectors. *Adv. Space Res.* **17**, 111–115.

Spahn, F., Schmidt, J., Albers, N., Hörning, M., Makuch, M., Seiß, M., Kempf, S., Srama, R., Dikarev, V., Helfert, S., Moragas-Klostermeyer, G., Krivov, A.V., Sremčević, M., Tuzzolino, A.J., Economou, T., Grün, E., 2006. Cassini Dust Measurements at Enceladus and Implications for the Origin of the E Ring. *Science* **311**, 1416–1418.

Spahn, F., Thiessenhusen, K.U., Colwell, J.E., Srama, R., Grün, E., 1999. Dynamics of dust ejected from Enceladus: Application to the Cassini dust detector. *J. Geophys. Res.* **104**, 24111–24120.

Srama, R., 2000. CDA calibration report. Technical Report. MPI-K.

Srama, R., 2010. Cassini–Huygens and Beyond – Tools for Dust Astronomy. Habilitation. Universität Stuttgart.

Srama, R., Ahrens, T.J., Altobelli, N., Auer, S., Bradley, J.G., Burton, M., Dikarev, V.V., Economou, T., Fechtig, H., Görlich, M., Grande, M., Graps, A., Grün, E., Havnes, O., Helfert, S., Horanyi, M., Igenbergs, E., Jessberger, E.K., Johnson, T.V., Kempf, S., Krivov, A.V., Krüger, H., Mocker-Ahlreep, A., Moragas-Klostermeyer, G., Lamy, P., Landgraf, M., Linkert, D., Linkert, G., Lura, F., McDonnell, J.A.M.,

B. Published literature that would be applicable to understanding the data or its processing

Möhlmann, D., Morfill, G.E., Müller, M., Roy, M., Schäfer, G., Schlotzhauer, G., Schwehm, G.H., Spahn, F., Stübig, M., Svestka, J., Tschernjawski, V., Tuzzolino, A.J., Wäsch, R., Zook, H.A., 2004. The Cassini Cosmic Dust Analyzer. *Space Science Reviews* **114**, 465–518.

Srama, R., Kempf, S., Moragas-Klostermeyer, G., Helfert, S., Ahrens, T.J., Altobelli, N., Auer, S., Beckmann, U., Bradley, J.G., Burton, M., Dikarev, V.V., Economou, T., Fechtig, H., Green, S.F., Grande, M., Havnes, O., Hillier, J.K., Horanyi, M., Igenbergs, E., Jessberger, E.K., Johnson, T.V., Krüger, H., Matt, G., McBride, N., Mocker, A., Lamy, P., Linkert, D., Linkert, G., Lura, F., McDonnell, J.A.M., Möhlmann, D., Morfill, G.E., Postberg, F., Roy, M., Schwehm, G.H., Spahn, F., Svestka, J., Tschernjawski, V., Tuzzolino, A.J., Wäsch, R., Grün, E., 2006. In situ dust measurements in the inner Saturnian system. *Planet. Space Sci.* **54**, 967–987.

Srama, R., Stephan, T., Grün, E., Pailer, N., Kearsley, A., Graps, A., Laufer, R., Ehrenfreund, P., Altobelli, N., Altwegg, K., Auer, S., Baggaley, J., Burchell, M.J., Carpenter, J., Colangeli, L., Esposito, F., Green, S.F., Henkel, H., Horanyi, M., Jäckel, A., Kempf, S., McBride, N., Moragas-Klostermeyer, G., Krüger, H., Palumbo, P., Srowig, A., Trieloff, M., Tsou, P., Sternovsky, Z., Zeile, O., Röser, H., 2009. Sample return of interstellar matter (SARIM). *Experimental Astronomy* **23**, 303–328.

Stübig, M., 2002. New insights in impact ionization and in time-of-flight mass spectroscopy with micrometeoroid detectors by improved impact simulations in the laboratory. Ph.D. thesis. Heidelberg University.

Stübig, M., Schäfer, G., Ho, T.M., Srama, R., Grün, E., 2001. Laboratory simulation improvements for hypervelocity micrometeorite impacts with a new dust particle source. *Planet. Space Sci.* **49**, 853–858.

C. CDA PDS data

Volume name	Start Time	End Time
COCDA_0001	1999-085	2000-100
COCDA_0002	2000-100	2001-100
COCDA_0003	2001-100	2002-100
COCDA_0004	2002-100	2003-100
COCDA_0005	2003-100	2003-300
COCDA_0006	2004-275	2004-366
COCDA_0007	2005-001	2005-090
COCDA_0008	2003-300	2004-100
COCDA_0009	2004-101	2004-200
COCDA_0010	2004-201	2004-274
COCDA_0011	2005-091	2005-181
COCDA_0012	2005-182	2005-202
COCDA_0013	2005-203	2005-233
COCDA_0014	2005-234	2005-273
COCDA_0015	2005-274	2005-290
COCDA_0016	2005-291	2005-310
COCDA_0017	2005-311	2005-330
COCDA_0018	2005-331	2005-365
COCDA_0019	2006-001	2006-030
COCDA_0020	2006-031	2006-060
COCDA_0021	2006-061	2006-090
COCDA_0022	2006-091	2006-121
COCDA_0023	2006-122	2006-152
COCDA_0024	2006-153	2006-181
COCDA_0025	2006-182	2006-212
COCDA_0026	2006-213	2006-243
COCDA_0027	2006-244	2006-273
COCDA_0028	2006-274	2006-304
COCDA_0029	2006-305	2006-335
COCDA_0030	2006-336	2006-365
COCDA_0031	2007-001	2007-031
COCDA_0032	2007-032	2007-062
COCDA_0033	2007-063	2007-090

Table C.1.: CDA data delivered to the PDS. The data can be downloaded from the website of the PDS small body node.

Volume name	Start Time	End Time
COCDA_0034	2007-091	2007-121
COCDA_0035	2007-122	2007-152
COCDA_0036	2007-153	2007-181
COCDA_0037	2007-182	2007-212
COCDA_0038	2007-213	2007-242
COCDA_0039	2007-243	2007-273
COCDA_0040	2007-274	2007-304
COCDA_0041	2007-305	2007-335
COCDA_0042	2007-336	2007-365
COCDA_0043	2008-001	2008-030
COCDA_0044	2008-031	2008-061
COCDA_0045	2008-062	2008-091
COCDA_0046	2008-092	2008-122
COCDA_0047	2008-123	2008-153
COCDA_0048	2008-154	2008-182
COCDA_0049	2008-183	2008-213
COCDA_0050	2008-214	2008-244
COCDA_0051	2008-245	2008-274
COCDA_0052	2008-275	2008-305
COCDA_0053	2008-306	2008-366
COCDA_0054	2009-001	2009-090
COCDA_0055	2009-091	2009-181
COCDA_0056	2009-182	2009-273
COCDA_0057	2009-274	2009-365
COCDA_0058	2010-001	2010-090
COCDA_0059	2010-091	2010-181
COCDA_0060	2010-182	2010-273
COCDA_0061	2010-274	2010-365

Table C.1.: CDA data delivered to the PDS. The data can be downloaded from the website of the PDS small body node.

D. CDA PDS product column description

D.1. Cassini CDA Area Table

#	Name	Units	Description
1	SENSOR AXIS ANGLE	°	This is the angle to the sensor axis where zero is along the axis.
2	IMPACT DE-TECTOR AREA	m^2	The exposed sensitive area of the CDA impact detector corresponding to the projected area of the hemispherical detector visible to an incoming particle traveling along a path at the SENSOR AXIS ANGLE.
3	CHEMICAL ANALYSER AREA	m^2	The exposed sensitive area of the CDA chemical analyser corresponding to the projected area of the hemispherical detector visible to an incoming particle traveling along a path at the SENSOR AXIS ANGLE.
4	TOTAL AREA	m^2	The total exposed sensitive area of the CDA corresponding to the projected area of the hemispherical detector visible to an incoming particle traveling along a path at the SENSOR AXIS ANGLE.

D.2. Cassini CDA Status History (CDA-STAT)

#	Name	Units	Description
1	EVENT TIME	UTC	The UTC time given in year, day of year, hours, minutes, and seconds in the general form: yyyy-dddThh:mm:ss.
2	LOCAL EVENT TIME	JD	The spacecraft event time given in year, day of year, hours, minutes, and seconds in the general form: yyyy-dddThh:mm:ss.

D. CDA PDS product column description

#	Name	Units	Description
3	EVENT DEFINI-TION		A five digit integer which indicates which detectors can trigger a particle detection, from left to right, Column Detector 1 QC 2 QA 3 QT 4 QI 5 QMA where the column value is 0 if the detector is switched off, and 1 if the detector is switched on.
4	QC THRESH-OLD SETTING		Code corresponding to the threshold setting at the time of impact for the amplifier connected to the chemical analyser target. Values are between 0 and 15. Conversion to Coulombs is dependent upon rise time and is found in CDASETTINGS.TAB.
5	QA THRESH-OLD SETTING		Code corresponding to the threshold setting at the time of impact for the amplifier connected to the chemical analyser grid. Values are between 0 and 15. Conversion to Coulombs is dependent upon rise time and is found in CDASET-TINGS.TAB.
6	QT THRESH-OLD SETTING		Code corresponding to the threshold setting at the time of impact for the amplifier connected to the impact ionization grid. Values are between 0 and 15. Conversion to Coulombs is dependent upon rise time and is found in CDASET-TINGS.TAB.
7	QI THRESH-OLD SETTING		Code corresponding to the threshold setting at the time of impact for the amplifier connected to the ion grid. Values are between 0 and 15. Conversion to Coulombs is dependent upon rise time and is found in CDASETTINGS.TAB.
8	QMA THRESH-OLD SETTING		Code corresponding to the threshold setting at the time of impact for the amplifier connected to the multiplier anode. Values are between 0 and 15. Conversion to Volts is found in CDASET-TINGS.TAB.
9	MULTIPLIER VOLTAGE LEVEL		The multiplier high voltage level setting, in steps between 0 and 255. Corresponding voltages are found in CDASETTINGS.TAB.
10	ION GRID VOLTAGE LEVEL		The ion grid high voltage level setting, in steps between 0 and 255. Corresponding voltages are found in CDASETTINGS.TAB.

D. CDA PDS product column description

#	Name	Units	Description
11	CHEMICAL ANALYSER VOLTAGE LEVEL		The chemical analyser high voltage level setting, in steps between 0 and 255. Corresponding voltages are found in CDASETTINGS.TAB.
12	CDA LISTEN FLAG		A flag indicating that CDA was in a measurement mode (1) or not (0).
13	CDA HARD STATUS		Code indicating whether CDA was on (1) or off (0).
14	CDA QI SHRINKING		A description of the degree of lossy data compression applied to the transmitted the time-resolved ion grid signal (QI), where there is no compression (1) or compression by factors of 2 (2) or 4 (4).
15	CDA QC SHRINKING		A description of the degree of lossy data compression applied to the transmitted time-resolved chemical analyzer target signal (QC), where there is no compression (1) or compression by factors of 2 (2) or 4 (4).
16	CDA QT SHRINKING		A description of the degree of lossy data compression applied to the transmitted time-resolved impact ionization target signal (QT), where there is no compression (1) or compression by factors of 2 (2) or 4 (4).
17	CDA QP SHRINKING		A description of the degree of lossy data compression applied to the transmitted time-resolved signal at the charge sensitive entrance grids (QP), where there is no compression (1) or compression by factors of 2 (2) or 4 (4).
18	CDA MP SHRINKING		A description of the degree of lossy data compression applied to the transmitted time-resolved time of flight mass spectrum (MP), where there is no compression (1) or compression by factors of 2 (2) or 4 (4).
19	CDA CONTENT CODE		A 20-bit integer describing which subset of the full event data set are downloaded.
20	CDA ARTICULATION POSITION	°	Deviation of the CDA axis about its mounting where 0 is defined as the position closest to the spacecraft axis and angle increases counter-clockwise from the mounting axis facing away from the spacecraft.

#	Name	Units	Description
21	CDA STATUS NOTE		Note concerning CDA or Cassini spacecraft status.

D.3. Cassini CDA Dust Analyser Event Table (CDA_DA_IMPACTS)

#	Name	Units	Description
1	IMPACT EVENT ID		An identifier number associated with a reliable impact.
2	IMPACT EVENT TIME	UTC	The UTC time of an event given in year, day of year, hours, minutes, and seconds in the general form: yyyy-dddThh:mm:ss. Uncertainty is about 1 second.
3	IMPACT EVENT JULIAN DATE	JD	The full Julian date of an impact event.
4	QP AMPLITUDE	C	The charge of the particle measured by the signal maximum of the entrance grid channel.
5	QP AMPLTUDE ERROR	C	The error associated with the QP amplitude.
6	QP SIGNAL-TO-NOISE RATIO		The signal-to-noise ratio associated with the entrance grid amplitude.
7	QI AMPLITUDE	C	Fraction of the plasma ion charge yield generated by the particle impact. The value is given by the maximum amplitude of the signal monitored by the integrating amplifier connected to the ion grid.
8	QI AMPLITUDE ERROR	C	The error associated with the QI amplitude.
9	QI SIGNAL-TO-NOISE RATIO		The signal-to-noise ratio associated with the ion channel amplitude.
10	QT AMPLITUDE	C	Fraction of the plasma electron charge yield generated by the particle impact. The value is given the maximum amplitude of the signal monitored by the integrating amplifier connected to the impact ionization target (IID).
11	QT AMPLITUDE ERROR	C	The error associated with the QT amplitude.

D. CDA PDS product column description

#	Name	Units	Description
12	QT SIGNAL-TO-NOISE RATIO		The signal-to-noise ratio associated with the impact ionization detector signal amplitude.
13	QC AMPLITUDE	C	Fraction of the electron charge yield generated by the particle impact. The value is given by the maximum amplitude of the signal monitored by the integrating amplifier connected to the chemical analyser target (CAT).
14	QC AMPLITUDE ERROR	C	The error associated with the QC amplitude.
15	QC SIGNAL-TO-NOISE RATIO		The signal-to-noise ratio associated with the chemical analyser target signal amplitude.
16	QI RISE TIME	s	The signal from the ion grid is reconstructed and converted to Coulomb. The rise time is that time elapsed between 10% and 90% of the signal maximum.
17	QI RISE TIME ERROR	s	The error associated with the ion grid signal rise time.
18	QT RISE TIME	s	The signal from the impact ionization detector is reconstructed and converted to Coulomb. The rise time is that time elapsed between 10% and 90% of the signal maximum.
19	QT RISE TIME ERROR	s	The error associated with the impact ionization detector signal rise time.
20	QC RISE TIME	s	The signal from the chemical analyzer target is reconstructed and converted to Coulomb. The rise time is that time elapsed between 10% and 90% of the signal maximum.
21	QC RISE TIME ERROR	s	The error associated with the rise time signal from the chemical analyzer target.
22	TARGET FLAG		The target flag (TF) indicates that portion of the target impacted. TF Portion UNKN Unknown CAT Chemical Analysis Target (inner target) IID Impact Ionization Detector (outer target) QPG Entrance Grid CATG Chemical Analyser Grid WA Wall impacts
23	SPACECRAFT RIGHT ASCENSION	°	The heliocentric right ascension (J2000) of the spacecraft.

D. CDA PDS product column description

#	Name	Units	Description
24	SPACECRAFT DECLINATION	°	The heliocentric declination (J2000) of the spacecraft.
25	SPACECRAFT-SUN DISTANCE	AU	The distance from the spacecraft to the sun.
26	SPACECRAFT SATURN SYSTEM III LONGITUDE	°	The sub-Saturn longitude of the spacecraft in the System III coordinates
27	SPACECRAFT SATURN SYSTEM III LATITUDE	°	The sub-Saturn latitude of the spacecraft in the System III coordinates.
28	SPACECRAFT-SATURN DISTANCE	RS	The distance from the spacecraft to Saturn.
29	SPACECRAFT X VELOCITY	$km\,s^{-1}$	The J2000 heliocentric equatorial X component of the Cassini velocity vector.
30	SPACECRAFT Y VELOCITY	$km\,s^{-1}$	The J2000 heliocentric equatorial Y component of the Cassini velocity vector.
31	SPACECRAFT Z VELOCITY	$km\,s^{-1}$	The J2000 heliocentric equatorial Z component of the Cassini velocity vector.
32	DETECTOR RIGHT ASCENSION	°	The spacecraft-centered right ascension (J2000) of the sensor axis.
33	DETECTOR DECLINATION	°	The spacecraft-centered declination (J2000) of the sensor axis.
34	COUNTER NUMBER		Event counter assigned by the on-board event evaluation algorithm with a value between 0 and 19. The event counter value is a rough measure for the properties of the registered event.
35	EVENT CLASS		Event class assigned by the on-board evaluation algorithm. The event class takes values between 0 and 3 and is a rough measure for the quality of the event (0 noise event candidate, 1 test pulse, 2 small impact, 3 strong impact, impacts with TOF mass spectrum)
36	PARTICLE SPEED	$km\,s^{-1}$	The impact speed of the particle relative to the spacecraft. When no speed can be determined, the value is set to -99.9.

#	Name	Units	Description
37	PARTICLE SPEED ERROR FACTOR		An upper and lower estimate of impactor speed relative to the spacecraft is obtained by multiplying and dividing, respectively, the particle speed by this factor. When no speed (hence error factor) can be determined, the value of this factor is set to -9.9.
38	PARTICLE MASS	kg	The particle mass. When the particle speed is not determined, the mass is not determined and is set to 0.e0.
39	PARTICLE MASS ERROR FACTOR		An upper and lower estimate of impactor mass is obtained by multiplying and dividing, respectively, the particle mass by this factor. When the speed is not determined, neither is the mass, and this factor is set to-9.9.
40	QUALITY FLAG		Definition TBD - 1.0 is excellent, 0.0 is poor.
41	PARTICLE CHARGE	C	The charge of a particle. When no charge can be determined, the value is set to 0.
42	PARTICLE CHARGE ERROR	C	The error associated with the particle charge.
43	SOURCE FLAG		A flag (SF) indicating the possible origin of the impacting particle: SF Source 0 Unknown 1 Interplanetary 2 Jupiter Dust Stream 3 Interstellar 4 Dust stream of unknown origin
44	SPECTRUM FLAG		A flag indicating if there exists a corresponding mass spectrum for the particle (1) or not (0).

D.4. Cassini CDA Spectra Peaks Table (CDA-SPECTRA-XXXXXXX)

Identified mass lines of event # XXXXXXX

#	Name	Units	Description
1	IMPACT EVENT ID		An identifier number associated with a reliable impact.
2	NUMBER PEAKS		The number of distinguishable peaks in the mass spectrum of an impacting particle.

D. CDA PDS product column description

#	Name	Units	Description
3	IMPACT TRIGGER OFFSET TIME	s	The estimated time between actual particle impact and the triggering of the Mass Analyser.
4	PEAK 1 FLIGHT TIME	s	Time elapsed between Mass Analyser triggering and first spectral peak.
5	PEAK 1 FLIGHT TIME UNCERTAINTY	s	The uncertainty in the time elapsed between Mass Analyser triggering and first spectral peak.
6	PEAK 1 AMPLITUDE	V	This is the peak amplitude in volts at the multiplier. The peak amplitude is determined in the processed data.
7	PEAK 1 INTEGRAL	V s	The peak integral is area below the amplitude curve. The integral is calculated on the processed data (x = time scale, y = volt-scale).
8	PEAK 1 SNR		Signal-to-noise ratio of first peak integral.
9	PEAK 1 MASS	amu	Atomic weight corresponding to 1st mass peak.
⋮			
71	PEAK 12 FLIGHT TIME	s	Time elapsed between Mass Analyser triggering and twelfth spectral peak.
72	PEAK 12 FLIGHT TIME UNCERTAINTY	s	The uncertainty in the time elapsed between Mass Analyser triggering and twelfth spectral peak.
73	PEAK 12 AMPLITUDE	V	This is the peak amplitude in volts at the multiplier. The peak amplitude is determined in the processed data.
74	PEAK 12 INTEGRAL	V s	The peak integral is area below the amplitude curve. The integral is calculated on the processed data (x = timescale, y = volt-scale).
75	PEAK 12 SNR		Signal-to-noise ratio of twelfth peak integral.
76	PEAK 12 MASS	amu	Atomic weight corresponding to 12th mass peak.

D.5. MP Signal Table (MS-XXXXXXX)

MP signal (TOF spectrum) of event # XXXXXXX

#	Name	Units	Description
1	TIME AFTER EVENT TRIGGERING	μs	Flight time measured from estimated time of impact.

#	Name	Units	Description
2	AMPLITUDE	V	Signal value provided by the multiplier channel

D.6. QI Signal Table (QI-XXXXXXX)

QI signal of event # XXXXXXX

#	Name	Units	Description
1	TIME AFTER EVENT TRIG-GERING	μs	Time elapsed after event triggering
2	QI amplitude	C	Impact charge measured at the ion collector

D.7. QT Signal Table (QT-XXXXXXX)

QT signal of event # XXXXXXX

#	Name	Units	Description
1	TIME AFTER EVENT TRIG-GERING	μs	Time elapsed after event triggering
2	QT amplitude	C	Electron charge signal monitored at the IID target generated by an impact

D.8. QC Signal Table (QC-XXXXXXX)

QC signal of event # XXXXXXX

#	Name	Units	Description
1	TIME AFTER EVENT TRIG-GERING	μs	Time elapsed after event triggering
2	QC amplitude	C	Ion charge signal monitored at the CAT target generated by an impact

D.9. CDA QP Signal Table (QP-XXXXXXX)

QP Charge Grid signal of event # XXXXXXX

#	Name	Units	Description
1	TIME BEFORE AND AFTER EVENT TRIGGERING	μs	Time measured from estimated impact time. Negative time values correspond to time values before the impact time, positive values after the impact time
2	QP amplitude	C	Charge induced by the dust particle at the charge grid device

D.10. Cassini CDA Settings Table

#	Name	Units	Description
1	QC THRESHOLD SETTING		Code corresponding to the threshold setting for the amplifier connected to the chemical analyzer target. Values are between 0 and 15
2	QC THRESHOLD SETTING COULOMB	C	Value in Coulombs corresponding to the code value
3	QA THRESHOLD SETTING		Code corresponding to the threshold setting for the amplifier connected to the chemical analyser grid. Values are between 0 and 15
4	QA THRESHOLD SETTING COULOMB	C	Value in Coulombs corresponding to the code value
5	QT THRESHOLD SETTING		Code corresponding to the threshold setting for the amplifier connected impact ionization target. Values are between 0 and 15
6	QT THRESHOLD SETTING	C	Value in Coulombs corresponding to the code value
7	QI THRESHOLD SETTING		Code corresponding to the threshold setting for the amplifier connected to the ion grid. Values are between 0 and 15
8	QI THRESHOLD SETTING COULOMB	C	Value in Coulombs corresponding to the code value
9	QMA THRESHOLD SETTING		Code corresponding to the threshold setting at the time of impact for the amplifier connected to the multiplier anode. Values are between 0 and 15

#	Name	Units	Description
. 10	QMA THRESH- OLD SETTING VOLTAGE	V	Value in Volts corresponding to the code value
11	MULTIPLIER VOLTAGE LEVEL		The multiplier high voltage level setting, in steps between 0 and 255.
12	MULTIPLIER VOLTAGE	V	Multiplier high voltage setting values
13	ION GRID VOLTAGE LEVEL		The ion grid high voltage level setting, in steps between 0 and 255.
14	ION GRID VOLTAGE	V	Ion grid high voltage setting values.
15	CHEMICAL ANALYSER VOLTAGE LEVEL		The chemical analyser high voltage level setting, in steps between 0 and 255.
16	CHEMICAL ANALYSER VOLTAGE	V	Chemical analyzer high voltage setting values

D.11. Cassini CDA Counter Table

#	Name	Units	Description
1	TIME		Time when the counter state snapshot was taken, given in UTC (years, hours, minutes, and seconds in the general form: yyyy-dddThh:mm:ss.) Uncertainty is about 1 second.
2	COUNTER 0		State of counter 0 at the time of the snapshot
3	COUNTER 1		State of counter 1 at the time of the snapshot
⋮			
27	COUNTER 25		State of counter 25 at the time of the snapshot
28	COUNTER 26		State of counter 26 at the time of the snapshot

E. IDL package for reading CDA PDS tables

pds_readTable.pro

```
 1  FUNCTION pds_cleanString , str , CLEAN = CLEAN
 2      ;;
 3      ;;
 4      ;;
 5      str = STRTRIM( str , 2)
 6      IF (STRPOS( str , '"') EQ 0) THEN str = STRMID( str , 1)
 7      IF ((p = STRPOS( str , '"')) NE −1) THEN str = STRMID( str , 0, p)
 8
 9      IF (NOT KEYWORD_SET(CLEAN)) THEN RETURN, str
10
11      WHILE(( p = STRPOS( str , '/')) NE −1) DO BEGIN
12          STRPUT, str , '_', p
13      ENDWHILE
14
15      WHILE(( p = STRPOS( str , ' ')) NE −1) DO BEGIN
16          STRPUT, str , '_', p
17      ENDWHILE
18
19      WHILE(( p = STRPOS( str , '−')) NE −1) DO BEGIN
20          STRPUT, str , '_', p
21      ENDWHILE
22
23      RETURN, str
24  END
25
26  FUNCTION pds_leapYear , year
27      ;;
28      ;;
29      ;;
30      d_this_year = (JULDAY(1, 1, year     ) + 1) MOD 7
31      d_next_year = (JULDAY(1, 1, year + 1) + 1) MOD 7
32      RETURN, (( d_next_year − d_this_year + 7) MOD 7) NE 1
33  END
34
35  PRO pds_doy2date , doy, day, month, year
36      ;;
37      ;;
38      ;;
39      doy_month = [31, 28, 31, 30,  31, 30, 31, 31, 30, 31, 30, 31]
```

```idl
40
41     ;; check for leap year
42     IF(pds_leapYear(year)) THEN doy_month[1] = 29
43
44     month = 1 & day = doy
45     WHILE (day GT doy_month[month-1]) DO BEGIN
46         day   = day - doy_month[month-1]
47         month = month + 1
48     ENDWHILE
49 END
50
51 FUNCTION pds_utc2jd, utc
52     ;;
53     ;;
54     ;;
55     IF(utc EQ '') THEN RETURN, 0.D
56
57     date = STRMID(utc, 0, (p = STRPOS(utc,'T')))
58     time = STRMID(utc, p+1)
59
60     time = STRSPLIT(time, '.', /EXTRACT)
61     time = FIX(STRSPLIT(time[0], ':', /EXTRACT))
62
63     date = FIX(STRSPLIT(date, '-', /EXTRACT))
64     IF(N_ELEMENTS(date) EQ 2) THEN BEGIN
65         pds_doy2date, date[1], day, month, date[0]
66         jd = JULDAY(month, day, date[0], time[0], time[1], time[2])
67     ENDIF ELSE BEGIN
68         jd = JULDAY(date[1], date[2], date[0], time[0], time[1], time
               [2])
69     ENDELSE
70
71     IF(N_ELEMENTS(time) GT 1) THEN BEGIN
72         subsec = DOUBLE(time[1])
73         jd += subsec/(24.D*3600.D*1000.D)
74     ENDIF
75
76     RETURN, jd
77 END
78
79 FUNCTION pds_readTableStructure, table
80     ;;
81     ;;
82     ;;
83     OPENR, unit, table, /GET_LUN
84
85      str = ''
86     WHILE(NOT EOF(unit)) DO BEGIN
87         READF, unit, str
88         IF(STRPOS(str, 'OBJECT') EQ -1) THEN CONTINUE
89
```

```idl
90          IF (STRPOS( str , 'HEADER' ) NE -1) THEN BEGIN
91              tabDef = { type :        'H' , $
92                          rows :        1L , $
93                          mt :          '' , $
94                          name :        ''}
95          tabStr = N_ELEMENTS( tabStr ) EQ 0 ? $
96                      [ tabDef ] : [ tabStr , tabDef ]
97          WHILE(NOT EOF( unit )) DO BEGIN
98              READF, unit , str
99              IF (STRPOS( str , 'END_OBJECT' ) NE -1) THEN BREAK
100         ENDWHILE
101      ENDIF
102
103      IF (STRPOS( str , 'TABLE' ) NE -1) THEN BEGIN
104          tabDef = { type :        'T' , $
105                      rows :        0L , $
106                      fmt :         '' , $
107                      name :        ''}
108         WHILE(NOT EOF( unit )) DO BEGIN
109             READF, unit , str
110             IF (STRPOS( str , 'END_OBJECT' ) NE -1) THEN BEGIN
111                 tabStr = N_ELEMENTS( tabStr ) EQ 0 ?   $
112                             [ tabDef ] : [ tabStr , tabDef ]
113                 BREAK
114             ENDIF
115
116             s = STRSPLIT( str , '=' , /EXTRACT)
117             IF (STRPOS( str , 'ROWS' ) NE -1) THEN BEGIN
118                 tabDef.rows = LONG( s [ 1 ] )
119             ENDIF ELSE $
120             IF (STRPOS( str , 'STRUCTURE' ) NE -1) THEN BEGIN
121                 tabDef.fmt = pds_cleanString ( s [ 1 ] )
122             ENDIF ELSE $
123             IF (STRPOS( str , 'NAME' ) NE -1) THEN BEGIN
124                 tabDef.name = pds_cleanString ( s [ 1 ] )
125             ENDIF
126         ENDWHILE
127      ENDIF
128  ENDWHILE
129
130  RETURN, tabStr
131 END
132
133 FUNCTION pds_readLabel , table , rowLength
134     ;;
135     ;;
136     ;;
137     OPENR, unit , table , /GET_LUN
138
139     str = ''
140     WHILE(NOT EOF( unit )) DO BEGIN
```

```idl
141         READF, unit, str
142         IF (STRPOS(str, 'RECORD_BYTES') NE -1) THEN BEGIN
143             rowLength = STRMID(str, STRPOS(str, '=') + 1)
144         ENDIF
145         IF (STRPOS(str, 'OBJECT') EQ -1) THEN CONTINUE
146         IF (STRPOS(str, 'COLUMN') EQ -1) THEN CONTINUE
147
148         colObj = {name:          '',                       $
149                   dataType:      -1,                       $
150                   number:        -1,                       $
151                   startByte:     -1,                       $
152                   bytes:          0,                       $
153                   format:        '',                       $
154                   unit:          '',                       $
155                   description:   ''}
156     WHILE(NOT EOF(unit)) DO BEGIN
157         READF, unit, str
158         IF (STRPOS(str, 'END_OBJECT') NE -1) THEN BEGIN
159             BREAK
160         ENDIF
161
162         s = STRSPLIT(str, '=', /EXTRACT)
163         IF (STRPOS(str, 'NAME') NE -1) THEN BEGIN
164             colObj.name = pds_cleanString(s[1], /CLEAN)
165         ENDIF ELSE                                         $
166         IF (STRPOS(str, 'DATA_TYPE') NE -1) THEN BEGIN
167             CASE pds_cleanString(s[1]) OF
168                 'ASCII_INTEGER':  colObj.dataType = 1
169                 'ASCII_REAL':     colObj.dataType = 2
170                 'CHARACTER':      colObj.dataType = 3
171                 'TIME':           colObj.dataType = 4
172                 ELSE: BEGIN
173                     print, 'MISSING DATA TYPE DEFINITION FOR ' +   $
174                             pds_cleanString(s[1])
175                 END
176             ENDCASE
177         ENDIF ELSE                                         $
178         IF (STRPOS(str, 'COLUMN_NUMBER') NE -1) THEN BEGIN
179             colObj.number = FIX(s[1])
180         ENDIF ELSE                                         $
181         IF (STRPOS(str, 'START_BYTE') NE -1) THEN BEGIN
182             colObj.startByte = FIX(s[1])
183         ENDIF ELSE                                         $
184         IF (STRPOS(str, 'BYTES') NE -1) THEN BEGIN
185             colObj.bytes = FIX(s[1])
186         ENDIF ELSE                                         $
187         IF (STRPOS(str, 'FORMAT') NE -1) THEN BEGIN
188             colObj.format = pds_cleanString(s[1])
189         ENDIF ELSE                                         $
190         IF (STRPOS(str, 'UNIT') NE -1) THEN BEGIN
191             colObj.unit = pds_cleanString(s[1])
```

```idl
192            ENDIF ELSE                                              $
193            IF(STRPOS(str, 'DESCRIPTION') NE -1) THEN BEGIN
194                s = STRMID(STRTRIM(STRMID(str, STRPOS(str, '=')+1), 2),
                       1)
195                IF((p = STRPOS(s, '"')) NE -1) THEN BEGIN
196                    colObj.description = STRMID(s, p)
197                ENDIF ELSE BEGIN
198                    colObj.description = s
199                    WHILE(NOT EOF(unit)) DO BEGIN
200                        READF, unit, str
201                        s = STRTRIM(str, 2)
202                        IF((p = STRPOS(s, '"')) NE -1) THEN           $
203                            s = STRMID(s, p)
204                        colObj.description += s
205                        IF(p NE -1) THEN BREAK
206                    ENDWHILE
207                ENDELSE
208            ENDIF
209        ENDWHILE
210        colDesc = N_ELEMENTS(colDesc) EQ 0 ?                          $
211                    [colObj] : [colDesc, colObj]
212    ENDWHILE
213
214    FREE_LUN, unit
215
216    RETURN, colDesc
217 END
218
219 FUNCTION pds_dataType2Data, dataType, TIME_STR = TIME_STR
220    ;;
221    ;;
222    ;;
223    CASE dataType OF
224        1: RETURN, 0L
225        2: RETURN, 0.D
226        3: RETURN, ''
227        4: RETURN, KEYWORD_SET(TIME_STR) ? '' : 0.D
228        ELSE: RETURN, 0
229    ENDCASE
230
231 END
232
233 PRO pds_rereadRow, unit, readIn, colDsc, rowLength
234    ;;
235    ;;
236    ;;
237    POINT_LUN, -unit, pos
238    POINT_LUN, unit, pos-rowLength
239
240    str = ''
241    READF, unit, str
```

```
242
243  FOR i = 0, N_ELEMENTS(colDsc)-1 DO BEGIN
244      fmt = '(T' + STRTRIM(colDsc[i].startByte, 2) + ',' + $
245                          colDsc[i].format + ')'
246      ON_IOERROR, badFormat
247      READS, str, (x = readIn.(i)), FORMAT = fmt
248      readIn.(i) = x
249      badFormat:
250  ENDFOR
251 END
252
253 FUNCTION pds_readTable, table, COLDESC = COLDSC
254      ;;
255      ;;
256      ;;
257      IF(N_ELEMENTS(table) LE 0) THEN BEGIN
258          table = DIALOG_PICKFILE(FILTER = ['*.LBL','*.TAB'])
259
260          IF(table EQ '') THEN RETURN, -1
261      END
262      IF((p = STRPOS(table, '.LBL')) NE -1) THEN BEGIN
263          name = STRMID(table, 0, p)
264      ENDIF ELSE IF((p = STRPOS(table, '.TAB')) NE -1) THEN BEGIN
265          name = STRMID(table, 0, p)
266      ENDIF ELSE RETURN, -1
267
268      lbl = name + '.LBL'
269      tab = name + '.TAB'
270      IF(FILE_TEST(lbl)) THEN BEGIN
271          colDsc = pds_readLabel(table, rowLength)
272          tabStr = pds_readTableStructure(table)
273      ENDIF ELSE BEGIN
274          print, 'LBL FILE DOES NOT EXIST!'
275          RETURN, -1
276      ENDELSE
277
278      ;; build structure for storing a row of the table object
279      ;;
280      readIn = CREATE_STRUCT(colDsc[0].name,                        $
281                          pds_dataType2Data(colDsc[0].dataType,  $
282                                          /TIME_STR))
283      FOR i = 1, N_ELEMENTS(colDsc)-1 DO BEGIN
284          readIn = CREATE_STRUCT(readIn, colDsc[i].name,           $
285                          pds_dataType2Data(colDsc[i].dataType,  $
286                                          /TIME_STR))
287      ENDFOR
288
289      ;; build format string for transforming the row data
290      ;;
291      format = 'T' + STRTRIM(colDsc[0].startByte, 2) + ',' +       $
292              colDsc[0].format
```

```idl
293    FOR i = 1, (nCols = N_ELEMENTS(colDsc))-1 DO BEGIN
294       format += ',T' + STRTRIM(colDsc[i].startByte, 2) + ',' +   $
295                 colDsc[i].format
296    ENDFOR
297    fmt = colDsc[nCols-1].format
298
299    IF (FILE_TEST(tab) NE 1) THEN BEGIN
300       tab = DIALOG_PICKFILE(TITLE = 'Locate data table!',      $
301                             FILTER = '*.tab')
302
303       IF (tab EQ '') THEN RETURN, -1
304    ENDIF
305
306    OPENR, unit, tab, /GET_LUN
307
308    str = ''
309    FOR i = 0L, N_ELEMENTS(tabStr)-1 DO BEGIN
310       CASE tabStr[i].type OF
311          'H': READF, unit, str
312          'T': BEGIN
313             data1 = REPLICATE(readIn, tabStr[i].rows)
314             POINT_LUN, -unit, posStart
315             FOR j = 0L, tabStr[i].rows-1 DO BEGIN
316                IF (EOF(unit)) THEN BEGIN
317                   PRINT, 'TABLE LENGTH INCONSITENT WITH LBL-FILE'
318                   FREE_LUN, unit
319                   RETURN, data
320                ENDIF
321                ON_IOERROR, badFormat
322                READF, unit, readIn, FORMAT = '(' + format + ')'
323                data1[j] = readIn
324                CONTINUE
325
326                badFormat: BEGIN
327                   MESSAGE, 'BAD FORMAT IN ROW ' + STRTRIM(j, 2), /
                         CONTINUE
328                   pds_rereadRow, unit, readIn, colDsc, rowLength
329                   data1[j] = readIn
330                   CONTINUE
331                END
332             ENDFOR
333          END
334       ENDCASE
335    ENDFOR
336
337    FREE_LUN, unit
338
339    iConvert = WHERE(colDsc.dataType EQ 4, nConvert)
340
341    IF (nConvert EQ 0) THEN RETURN, data1
342
```

```
343     rowDef = CREATE_STRUCT( colDsc [ 0 ] . name ,                          $
344                              pds_dataType2Data ( colDsc [ 0 ] . dataType ) )
345     FOR i = 1, N_ELEMENTS( colDsc )−1 DO BEGIN
346        rowDef = CREATE_STRUCT( rowDef ,  colDsc [ i ] . name ,             $
347                              pds_dataType2Data ( colDsc [ i ] . dataType ) )
348     ENDFOR
349
350     data = REPLICATE( rowDef ,  N_ELEMENTS( data1 ) )
351     FOR i = 0, N_ELEMENTS( colDsc )−1 DO BEGIN
352        IF ( colDsc [ i ] . dataType NE 4) THEN BEGIN
353           data . ( i ) = data1 . ( i )
354        ENDIF ELSE BEGIN
355           FOR j = 0L, N_ELEMENTS( data )−1 DO BEGIN
356              data [ j ] . ( i ) = pds_utc2jd ( data1 [ j ] . ( i ) )
357           ENDFOR
358        ENDELSE
359     ENDFOR
360
361     RETURN, data
362 END
363
364 PRO pds_readStream ,  tabStr ,  unit ,  path ,  data
365     ; ;
366     ; ;
367     ; ;
368     fmt = path + '/' + tabStr . fmt
369     IF ( FILE_TEST ( fmt ) NE 1) THEN BEGIN
370        PRINT,  'FMT FILE DOES NOT EXIST! '
371        RETURN
372     ENDIF
373
374     colDsc = pds_readLabel ( fmt )
375
376     ; ; build structure for storing a row of the table object
377     ; ;
378     readIn = CREATE_STRUCT( colDsc [ 0 ] . name ,                          $
379                             pds_dataType2Data ( colDsc [ 0 ] . dataType ,  $
380                                               /TIME_STR ) )
381     FOR i = 1, N_ELEMENTS( colDsc )−1 DO BEGIN
382        readIn = CREATE_STRUCT( readIn ,  colDsc [ i ] . name ,            $
383                             pds_dataType2Data ( colDsc [ i ] . dataType ,  $
384                                               /TIME_STR ) )
385     ENDFOR
386
387     ; ; build format string for transforming the row data
388     ; ;
389     format = 'T' + STRTRIM( colDsc [ 0 ] . startByte ,  2) + ',' +        $
390              colDsc [ 0 ] . format
391     FOR i = 1, N_ELEMENTS( colDsc )−1 DO BEGIN
392        format += ',T' + STRTRIM( colDsc [ i ] . startByte ,  2) + ',' +   $
393                 colDsc [ i ] . format
```

```idl
394        ENDFOR
395
396        str = ''
397        data = REPLICATE(readIn, tabStr.rows)
398        FOR j = 0L, tabStr.rows-1 DO BEGIN
399            IF(EOF(unit)) THEN BEGIN
400                MESSAGE, 'TABLE LENGTH INCONSITENT WITH FMT-FILE', /
                        CONTINUE
401                FREE_LUN, unit
402                RETURN
403            ENDIF
404            ;print, STRTRIM(j, 2) + '/' + STRTRIM(tabStr.rows, 2)
405            READF, unit, readIn, FORMAT = '(' + format + ')'
406            data[j] = readIn
407        ENDFOR
408
409        help, data
410 END
411
412 PRO pds_readStreamTab, data1, data2, data3
413        ;;
414        ;;
415        ;;
416        IF(N_ELEMENTS(table) LE 0) THEN BEGIN
417            table = DIALOG_PICKFILE(FILTER = ['*.tab'], $
418                                    GET_PATH = path)
419
420            IF(table EQ '') THEN RETURN
421        END
422
423        str = ''
424        OPENR, unit, table, /GET_LUN
425        WHILE(NOT EOF(unit)) DO BEGIN
426            READF, unit, str
427
428            IF(STRPOS(str, 'OBJECT') NE -1) THEN BEGIN
429                tabDef = {rows:        1L,                                    $
430                          fmt:         '',                                    $
431                          name:        ''}
432
433                WHILE(NOT EOF(unit)) DO BEGIN
434                    READF, unit, str
435
436                    s = STRSPLIT(str,'=', /EXTRACT)
437                    IF(STRPOS(str, 'ROWS') NE -1) THEN BEGIN
438                        tabDef.rows = LONG(s[1])
439                    ENDIF ELSE $
440                    IF(STRPOS(str, 'STRUCTURE') NE -1) THEN BEGIN
441                        tabDef.fmt = pds_cleanString(s[1])
442                    ENDIF ELSE $
443                    IF(STRPOS(str, 'NAME') NE -1) THEN BEGIN
```

```
444                    tabDef.name = pds_cleanString(s[1])
445                ENDIF
446
447                IF (STRPOS(str, 'END_OBJECT') NE −1) THEN BEGIN
448                    tabStr = N_ELEMENTS(tabStr) EQ 0 ?                    $
449                        [tabDef] : [tabStr, tabDef]
450
451                    IF (NOT EOF(unit)) THEN  READF, unit, str
452                    BREAK
453                ENDIF
454            ENDWHILE
455        ENDIF
456        IF (STRPOS(str, 'END') NE −1) THEN BREAK
457    ENDWHILE
458
459    FOR i = 0, N_ELEMENTS(tabStr)−1 DO BEGIN
460        print, '*****', tabStr[i].name
461        pds_readStream, tabStr[i], unit, path, data
462
463        CASE i OF
464            0: data1 = data
465            1: data2 = data
466            2: data3 = data
467        ENDCASE
468    ENDFOR
469
470    FREE_LUN, unit
471
472    PRINT, 'DONE'
473 END
```